SISSA

Lyman-α constraints on warm and on warm-plus-cold dark matter models

To cite this article: Alexey Boyarsky *et al* JCAP05(2009)012

View the article online for updates and enhancements.

Lyman-α constraints on warm and on warm-plus-cold dark matter models

Alexey Boyarsky,[a,b] **Julien Lesgourgues,**[c,d,e] **Oleg Ruchayskiy**[c] **and Matteo Viel**[f,g]

[a]Institute for Theoretical Physics, ETH Zurich, Zürich, CH-8093, Switzerland

[b]Bogolyubov Institute for Theoretical Physics,
14-b, Metrolohichna str., Kiev 03680, Ukraine

[c]École Polytechnique Fédérale de Lausanne, FSB/BSP/ITP/LPPC,
CH-1015, Lausanne, Switzerland

[d]PH-TH, CERN, CH-1211 Geneve 23, Switzerland

[e]LAPTH, Université de Savoie, CNRS,
B.P.110, F-74941 Annecy-le-Vieux Cedex, France

[f]INAF — Osservatorio Astronomico di Trieste,
Via G.B. Tiepolo 11, I-34131 Trieste, Italy

[g]INFN — National Institute for Nuclear Physics,
Via Valerio 2, I-34127 Trieste, Italy

E-mail: boyarsky@mail.cern.ch, Julien.Lesgourgues@cern.ch,
oleg.ruchayskiy@epfl.ch, viel@oats.inaf.it

Abstract. We revisit Lyman-α bounds on the dark matter mass in Λ Warm Dark Matter (ΛWDM) models, and derive new bounds in the case of mixed Cold plus Warm models (ΛCWDM), using a set up which is a good approximation for several theoretically well-motivated dark matter models. We combine WMAP5 results with two different Lyman-α data sets, including observations from the Sloan Digital Sky Survey. We pay a special attention to systematics, test various possible sources of error, and compare the results of different statistical approaches. Expressed in terms of the mass of a non-resonantly produced sterile neutrino, our bounds read $m_{\mathrm{NRP}} \geq 8$ keV (frequentist 99.7% confidence limit) or $m_{\mathrm{NRP}} \geq 12.1$ keV (Bayesian 95% credible interval) in the pure ΛWDM limit. For the mixed model, we obtain limits on the mass as a function of the warm dark matter fraction F_{WDM}. Within the mass range studied here (5 keV $< m_{\mathrm{NRP}} < \infty$), we find that any mass value is allowed when $F_{\mathrm{WDM}} < 0.6$ (frequentist 99.7% confidence limit); similarly, the Bayesian joint probability on $(F_{\mathrm{WDM}}, 1/m_{\mathrm{NRP}})$ allows any value of the mass at the 95% confidence level, provided that $F_{\mathrm{WDM}} < 0.35$.

Contents

1 Introduction

The nature of Dark Matter (DM) is one of the most intriguing questions of particle astrophysics. Its resolution would have a profound impact on the development of particle physics beyond its Standard Model (SM). Although the possibility of having massive compact halo objects (MACHOs) as a dominant form of DM is still under debates (see recent discussion in [1] and references therein), it is widely believed that DM is made of non-baryonic particles. Yet the SM of elementary particles does not contain a viable DM particle candidate – a massive, neutral and stable (or at least cosmologically long-lived) particle. Active neutrinos, which are both neutral and stable, form structures in a top-down fashion [2–6], and thus cannot produce the observed large scale structure. Therefore, the DM particle hypothesis implies an extension of the SM. Thus, constraining the properties of DM helps to distinguish between various DM candidates and may help to differentiate among different models Beyond the Standard Model (BSM).

What is known about the properties of DM particles?

DM particle candidates may have very different masses (for reviews of DM candidates see e.g. [7–10]): massive gravitons with mass $\sim 10^{-19}$ eV [11], axions with mass $\sim 10^{-6}$ eV [12–14], sterile neutrinos with mass in the keV range [15], supersymmetric (SUSY) particles (gravitinos [16], neutralinos [17, 18], axinos [19, 20] with mass ranging from a few eV to hundreds GeV), supersymmetric Q-balls [21], WIMPZILLAs with mass $\sim 10^{13}$ GeV [22, 23], and many others. Thus, the mass of DM particles becomes an important characteristics which may help to distinguish between various DM candidates and, more importantly, may help to differentiate among different BSMs. A quite robust and model-independent *lower bound* on the mass of spin-one-half DM particles was suggested in [24]. The idea was based on the fact that for any fermionic DM the average phase-space density (in a given DM-dominated, gravitationally bound object) cannot exceed the phase-space density of the degenerate Fermi gas. This argument, applied to the most DM-dominated dwarf Spheroidal (dSph) satellites of the Milky Way leads to the bound $m_{\text{DM}} > 0.41$ keV [25]. For particular DM models (with known primordial velocity dispersion) and under certain assumptions about the evolution of the system during structure formation, this limit can be strengthened. This idea was developed in a number of works [25–34] (for recent results and a critical discussion see [25]).

For any DM candidate there should exist a production mechanism in the early Universe. Although it is possible that the DM is produced entirely through interactions with non-SM particles (e.g. from the inflaton decay) and is inert with respect to all SM interactions, many popular DM candidates are produced via interactions with the SM sector. One possible class of DM candidates are *weakly interacting massive particles* — WIMPs [17]. They have interactions with SM particles of roughly electroweak strength. The WIMPs are completely stable particles, as their interaction strength would otherwise imply a lifetime incompatible with a sizable relic density today. Therefore, they are produced in the early Universe via annihilation into SM particles with roughly weak interaction cross-section (see e.g. [35]). To have a correct abundance, these particles should have a mass in the GeV to TeV range. Such a mass and interaction strength means that they decouple from the primeval plasma deeply in the radiation dominated epoch, while being non-relativistic. Such particles have a Boltzmann velocity distribution function at the moment of freeze-out and are called "cold DM" (CDM). In the CDM scenario, structure formation goes in the bottom-up fashion: the smallest structures (with supposed masses as small as that of the Earth) form first, and then combined into larger structures.

Another wide class of DM candidates can be generically called *superweakly* interacting (see e.g. [36]), meaning that their cross-section of interaction with SM particles is much smaller than the weak one. There are many examples of *super-WIMP* DM models: sterile neutrinos [15], gravitinos in theories with broken R-parity [37, 38], light volume moduli [39] or Majorons [40]. Many of these candidates (e.g. sterile neutrino, gravitino, Majoron) possess a two-body decay channel: DM $\to \gamma + \nu, \gamma + \gamma$. These scenarios are very interesting, since apart from laboratory detection such particles can be searched in space. Looking for a monochromatic decay line in the spectra of DM-dominated objects provides a way of *indirect detection* of DM, and could help to *constrain* its interaction strength with SM particles. The astrophysical search for *decaying* DM is in fact more promising than for stable (annihilating) DM. Indeed, the decay signal is proportional to the *column density* $\int \rho_{\text{DM}}(r)dr$, i.e. the density integrated along the line of sight, and not the squared density $\int \rho_{\text{DM}}^2(r)dr$ (as it is the case for annihilating DM). As a consequence, *(i)* a vast variety of astrophysical objects of different nature would produce roughly the same decay signal [41, 42]; *(ii)* this gives more freedom for

choosing the observational targets, and avoid complicated astrophysical backgrounds (e.g. one does not need to look at the Galactic center, expecting a comparable signal from dark outskirts of galaxies, clusters and dark dSph's); *(iii)* if a candidate line is identified, its surface brightness profile may be measured (since it does not decay quickly away from the centers of objects), in order to distinguish it from astrophysical lines (which usually decay in outskirts) and to compare with the signal from several other objects. For all these reasons, astrophysical search for decaying DM can almost be viewed as another type of *direct detection*. A search for DM decay signals was conducted both in the keV — MeV range [41, 43–47] and GeV range [42].

The small strength of interaction of light super-WIMP particles usually implies that:

(i) they were never in thermal equilibrium in the early Universe; and

(ii) they were produced deep in the radiation dominated epoch, while still being relativistic (unlike CDM).

The latter property means that the density perturbation of these particles are suppressed for scales below their *free-streaming length*,[1] which affects structure formation on those scales. If the maximum free-streaming length roughly coincides with galaxy scales, the particles are called Warm Dark Matter (WDM), see e.g. [48].

Currently, the best way to distinguish between WDM and CDM models is the analysis of Lyman-α (Ly-α) forest data (for an introduction see e.g. [49–51]). This method requires particular care. Part of the physics entering into the Ly-α analysis is not fully understood (for a recent review see [52]), and can be significantly influenced by DM particles (see e.g. [53–59]). The results can also be affected by approximations related to computational difficulties. Indeed, at the redshifts probed by Ly-α data, structures are already undergoing non-linear evolution. In order to relate the measured flux spectrum with the parameters of each cosmological model, one would have to perform a prohibitively large number of numerical simulations. Therefore, various simplifying approximations have to be realized. Different approaches are presented in [60–62].

Previous works analyzing Ly-α constrains on WDM [63–66] assumed the simplest ΛWDM model with a cut-off in the linear power spectrum (PS) of matter density fluctuations. Such a PS arises when WDM particles are *thermal relics*. However, in many super-weakly interacting DM models, the PS has a complicated non-universal form due to the non-thermal primordial velocity distribution (see e.g. [67–70]). For example, in gravitino models with broken R-parity, gravitino production occurs in two stages: thermally at high temperatures (see e.g. [71–73]), and then non-thermally through the late decay of the next-to-lightest supersymmetric particle (see e.g. [67, 74]). Therefore the primordial velocity distribution results from the superimposition of a colder (resonant) and a warmer (thermal) component, and the PS is characterized by a step and a plateau on small scales (rather than a sharp cut-off).

Another interesting super-WIMP WDM model with a non-trivial PS is the sterile neutrino DM of the νMSM— an extension of the SM by three sterile (right-handed, gauge singlet) neutrinos [75, 76]. Having masses of all new particles below the electro-weak scale, this model is able to explain simultaneously three BSM phenomena:

(i) the transition between the neutrino of different flavours (*neutrino oscillations*);

---

[1]The free-streaming length is the equivalent of the Jeans length for a collisionless fluid. It is given by the ratio $\lambda_{\rm FS} \sim \langle v \rangle / H$, where $\langle v \rangle$ is the velocity dispersion of the particles.

(ii) the production of a non-zero baryon number in the early Universe; and

(iii) the existence of DM candidate with correct relic density.[2]

Sterile neutrino DM in the νMSM is produced via its mixing with active neutrinos in the early Universe [15, 78–81]. In the absence of lepton asymmetry, the production rate is strongly suppressed at temperatures above few hundreds of MeV and peaks roughly at $T_{\rm peak} \sim 130 \left(\frac{M_{\rm DM}}{1\,{\rm keV}}\right)^{1/3}$ MeV [15]. The resulting momentum distribution of sterile neutrino DM is approximately that of a rescaled Fermi-Dirac [15, 82], with its temperature equal to that of active neutrinos (see (2.1) below). We will call this production mechanism **NRP** — *non-resonant production*. Notice that this production channel is always present (although it may be subdominant, see below).

The sterile neutrino DM production changes in the presence of a lepton asymmetry [78]. In this case the dispersion relations for active and sterile neutrinos may cross each other. This results in an effective transfer of an excess of active neutrinos (or antineutrinos) to the population of DM sterile neutrinos. The lepton asymmetry necessary for this *resonant production* (**RP**) is generated via the decay of heavier sterile neutrinos [83]. In the RP scenario, for each mass and lepton asymmetry, the velocity dispersion has a colder (resonant) component and a warmer (non-resonantly produced) tail. For a recent review see e.g. [84].

Sterile neutrinos having colder and warmer velocity components can also be produced through the decay of a gauge-singlet scalar, followed by a subsequent non-resonant production [85–89]. The decay of this scalar field should occur at temperatures $\gtrsim 100\,{\rm GeV}$ and the produced sterile neutrinos do not share subsequent entropy releases [85, 87]. As a result the characteristic momentum of sterile neutrinos, produced in that way, is several times colder than the average momentum of the NRP component (see e.g. [85]). Notice that in this case the production is determined not only by the mixing between active and sterile neutrinos, but also by the coupling of the sterile neutrino with the scalar.

We see that in several well-motivated models, the primordial momentum distribution of DM particles contains a warm (Fermi-Dirac-like component) and a colder one. Therefore, in this work, apart from updating existing bounds on ΛWDM models, we consider Ly-α bounds in the $\Lambda CWDM$ scenario, including a mixture of a CDM and WDM. This model is characterized by two independent parameters beyond the usual dark matter fraction $\Omega_{\rm DM}$: the velocity dispersion (or free-streaming length) of the WDM component, and the fraction of WDM density. We will overview and provide a critical analysis of uncertainties in the Ly-α method for this model, and derive constraints on the above parameters. Finally, we will discuss the consequences of these results for some physically relevant DM models of this kind.

The first qualitative analysis of Ly-α bounds in the ΛCWDM scenario was performed in [90]. In this work, the authors computed the *linear* ΛCWDM power spectra projected along the line of sight. The PS suppression (as compared to the pure ΛCDM case) at some fiducial scale was compared with that quoted in [64] for several WDM masses. A ΛCWDM model was considered as ruled out at some confidence level if it produced the same suppression in the 1D projected linear PS as a pure ΛWDM model ruled out at the same level in [64].

This qualitative method should be improved in two directions. First of all, the Ly-α method provides a measurement of the 1D *non-linear* flux spectrum. The non-linear evolution "mixes" different scales. Therefore, two linear PS passing through the same point at a

---

[2]This model also eases the *hierarchy problem*, as the νMSM can be thought of as a consistent quantum field theory, valid all the way to the Planck scale. The hierarchy problem is then shifted into the realm of quantum gravity, broadly understood as a fundamental theory, superseeding at the Planck scale [77].

given wave number but having a different behavior otherwise would fit Ly-α data differently. Secondly, the effects of CWDM suppression on the matter PS can be somewhat compensated by the change of cosmological parameters (DM abundances, σ_8, etc.). Therefore, a proper Ly-α analysis should include a simultaneous fitting of all cosmological plus CWDM parameters to the Ly-α (and possibly other cosmological) data. Such an analysis is performed in this work.

The paper is organized as follows. In section 2, we describe the effect of a mixture of cold and warm dark matter on the linear matter power spectrum, and present some analytic approximations. In section 3, we introduce the two Ly-α data sets used in this analysis: the Viel, Haenelt & Springel (VHS) data compiled in ref. [91], and the Sloan Digital Sky Survey (SDSS) data complied in ref. [61, 92]. In section 4, we discuss the issue of including thermal velocities in hydrodynamical simulations in presence of warm dark matter. The reader only interested in our results could go directly to section 5, where we present the bounds based on the conservative VHS data set, and to section 6, which contains our analysis for the more constraining SDSS data. In section 7, we describe the systematic errors included in our analysis. Finally, in section 8, we discuss some implications of our results.

2 Linear power spectrum in CWDM models

The growth of matter density perturbations in the Universe is conveniently described in terms of a *power spectrum* $P(k) = \langle |\frac{\delta\rho_{\rm M}}{\rho_{\rm M}}|^2_k \rangle$ (where $\rho_{\rm M}$ is the matter density, and $< \cdot >$ denotes the ensemble average). The time evolution of this power spectrum from its primordial form (taken in this paper to be a power law with index n_s) to a redshift of interest depends on cosmological parameters (fraction of dark $\Omega_{\rm DM}$ and baryonic $\Omega_{\rm B}$ matter, Ω_Λ, Hubble constant, etc.)

Pure warm DM models contain another parameter which affects the evolution of density perturbations: the initial DM velocity dispersion. In this paper, for definiteness, we assume that the WDM component has a mass $m_{\rm NRP}$ and a primordial phase-space distribution $f(p)$ of the form

$$f(p) = \frac{\chi}{\exp(p/T_\nu) + 1} \ . \tag{2.1}$$

This form is motivated by the scenario of non-resonantly produced (NRP) sterile neutrinos [15, 82]. The temperature $T_\nu \equiv (4/11)^{1/3} T_\gamma$ is the temperature of active neutrinos in the instantaneous decoupling approximation, while the normalization parameter $\chi \ll 1$ is determined by the mass $m_{\rm NRP}$ and the requirement of a correct DM abundance.[3] Another well-motivated WDM model is that of *thermal relics* (TR). This is a generic name for particles that were in thermal equilibrium in the early Universe and decoupled while being relativistic (unlike sterile neutrinos which never equilibrated). In the TR case, the phase-space distribution is of the Fermi-Dirac type: namely, similar to equation (2.1) although χ is equal to one, and the temperature $T_{\rm TR}$ is not equal to T_ν but can be deduced from the mass of thermal relics $m_{\rm TR}$ and the DM abundance. At the level of linear perturbations, the NRP and TR models are formally equivalent under the identification $T_{\rm TR} = \chi^{1/4} T_\nu$ and mass $m_{\rm TR} = \chi^{1/4} m_{\rm NRP}$ [93].

To separate the influence of the velocity dispersion on the evolution of density perturbations, it is convenient to construct a *transfer function* — the square root of the ratio of the matter power spectrum of a given ΛWDM model to that of a pure ΛCDM with the same

---

[3]Eq. (2.1) is only an approximation to the real sterile neutrino DM spectrum, which can be computed only numerically (see [80] for details).

choice of cosmological parameters:

$$T(k) \equiv \left(\frac{P_{\Lambda\mathrm{WDM}}}{P_{\Lambda\mathrm{CDM}}} \right)^{1/2} . \tag{2.2}$$

This transfer function turns out to be rather insensitive to the values of cosmological parameters, and is well fitted by

$$T(k) = (1 + (k/k_0)^{2\nu})^{-5/\nu} , \tag{2.3}$$

where $\nu = 1.12$, and the scale k_0 (related to the free-steaming scale) is given as a function of the mass and cosmological parameters (see e.g. [63]). This function describes a cut-off with k^{-10} dependence on scales $k \gg k_0$.

In this paper we will consider a class of models where DM is a mixture of cold and warm (with velocity dispersion in the form (2.1)) components. We define the *WDM fraction* f_{WDM} as

$$f_{\mathrm{WDM}} \equiv \frac{\Omega_{\mathrm{WDM}}}{\Omega_{\mathrm{M}}}, \qquad \Omega_{\mathrm{M}} = \Omega_{\mathrm{CDM}} + \Omega_{\mathrm{WDM}} + \Omega_{\mathrm{B}} \tag{2.4}$$

(note the presence of the baryonic fraction Ω_{B} in the denominator). The transfer function of ΛCWDM models is qualitatively different. The characteristic behavior of the ΛCWDM power spectrum as compared to the pure ΛCDM one for the same cosmological parameters is shown on figures 1), (2, and can be summarized as follows:

– The scale where the transfer function departs from 1 depends on the mass m_{NRP} of the WDM component, but not on f_{WDM}, as figures 1 and 2 demonstrate.

– For large k's, the transfer function approaches a constant plateau. The height of this plateau is determined solely by f_{WDM}, as figure 2 demonstrates.

2.1 Characteristic scales

At any given time, the comoving free-streaming wavenumber of the warm component is defined as

$$k_{\mathrm{FS}} \equiv \sqrt{4\pi G \rho} \, \frac{a}{\langle v \rangle} = \sqrt{\frac{3}{2}} \frac{aH}{\langle v \rangle} \tag{2.5}$$

where ρ is the total density of the universe at the time considered, $\langle v \rangle$ is the velocity dispersion of the warm component only (not to be confused with the velocity dispersion of the total cold plus warm component, which depends on f_{WDM}), a is the scale factor and H the Hubble rate. This definition is analogous to that of the Jeans scale for a fluid. The wavenumber k_{FS} appears in the perturbation equations, and corresponds to the wavelength below which perturbations cannot experience gravitational collapse due to their velocity dispersion. In the radiation era, when the fluid is ultra-relativistic, $\langle v \rangle \simeq 1$ (using units where $c = 1$) and k_{FS} evolves like the comoving Hubble scale, $k_{\mathrm{FS}} = \sqrt{3/2} \, aH \propto t^{-1/2}$. After the non-relativistic transition, $\langle v \rangle = \langle p \rangle / m$ scales like a^{-1}; with our choice for $f(p)$, the average velocity is given approximately by $\langle v \rangle = 3T_\nu / m_{\mathrm{NRP}}$. Hence, during the rest of radiation domination, the comoving free-streaming scale remains constant with

$$k_{\mathrm{FS}} = \sqrt{4\pi G \rho_R} \, \frac{a m_{\mathrm{NRP}}}{3 T_\nu} = \sqrt{\frac{\Omega_R}{6}} H_0 \frac{m_{\mathrm{NRP}}}{T_\nu^0} = 7 \left(\frac{m_{\mathrm{NRP}}}{1 \, \mathrm{keV}} \right) \left(\frac{0.7}{h} \right) h/\mathrm{Mpc} \tag{2.6}$$
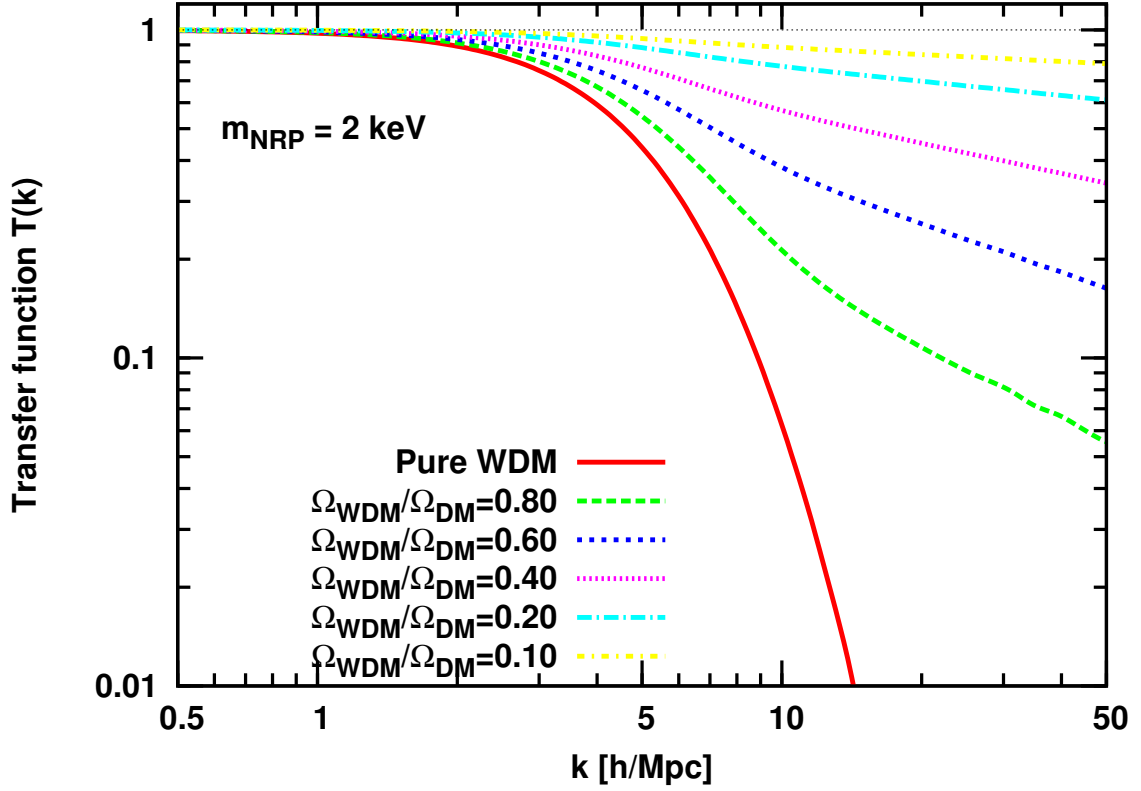
Figure 1. Transfer functions $T(k) \equiv [P_{\Lambda\text{CWDM}}(k)/P_{\Lambda\text{CDM}}(k)]^{1/2}$ for $m_{\text{NRP}} = 2$ keV and different WDM fractions: from left to right, $\Omega_{\text{WDM}}/(\Omega_{\text{WDM}} + \Omega_{\text{CDM}}) = 1, 0.8, 0.6, 0.4, 0.2, 0.1$. Other parameters are fixed to $\Omega_{\text{B}} = 0.05$, $\Omega_{\text{M}} = 0.3$, $\Omega_{\Lambda} = 0.7$, $h = 0.7$.

where T_ν^0 is the current neutrino temperature, and we assumed the scale factor to be normalized to unity today. Later on, k_{FS} increases like $t^{1/3}$ during matter domination, and even faster during Λ domination. Today, assuming the universe to be flat, the free-streaming scale is equal to

$$k_{\text{FS}}^0 = \sqrt{4\pi G \rho_c^0} \, \frac{m_{\text{NRP}}}{3T_\nu^0} = \sqrt{\frac{1}{6}} H_0 \frac{m_{\text{NRP}}}{T_\nu^0} = 8 \times 10^2 \left(\frac{m_{\text{NRP}}}{1 \text{ keV}}\right) h/\text{Mpc} . \qquad (2.7)$$

Below this scale (for $k > k_{\text{FS}}$), perturbations can never experience gravitational clustering. Hence, this scale marks roughly the beginning of the region for which the free-streaming effect is maximal and the CWDM power spectrum is reduced by a constant amplitude (the plateau in figure 2).

By analogy with the case of light active neutrinos, one could expect that the minimum of the free-streaming scale $k_{\text{FS}}^{\text{min}}$ (eq. (2.6)) would give the point at which the ΛCWDM power spectrum starts to differ from the ΛCDM one. However, $k_{\text{FS}}^{\text{min}}$ does not give the right answer, as can be checked on figure figure 2. In fact, the largest scale affected by free-streaming is nothing but the present value of the particle horizon of warm particles with a typical velocity $\langle v \rangle$, that we will call the (comoving) free-streaming horizon λ_{FSH}

$$\lambda_{\text{FSH}}^0 = \int_0^{t_0} \frac{\langle v \rangle}{a} \, dt = \int_0^1 \frac{\langle v \rangle}{a^2 H} \, da . \qquad (2.8)$$
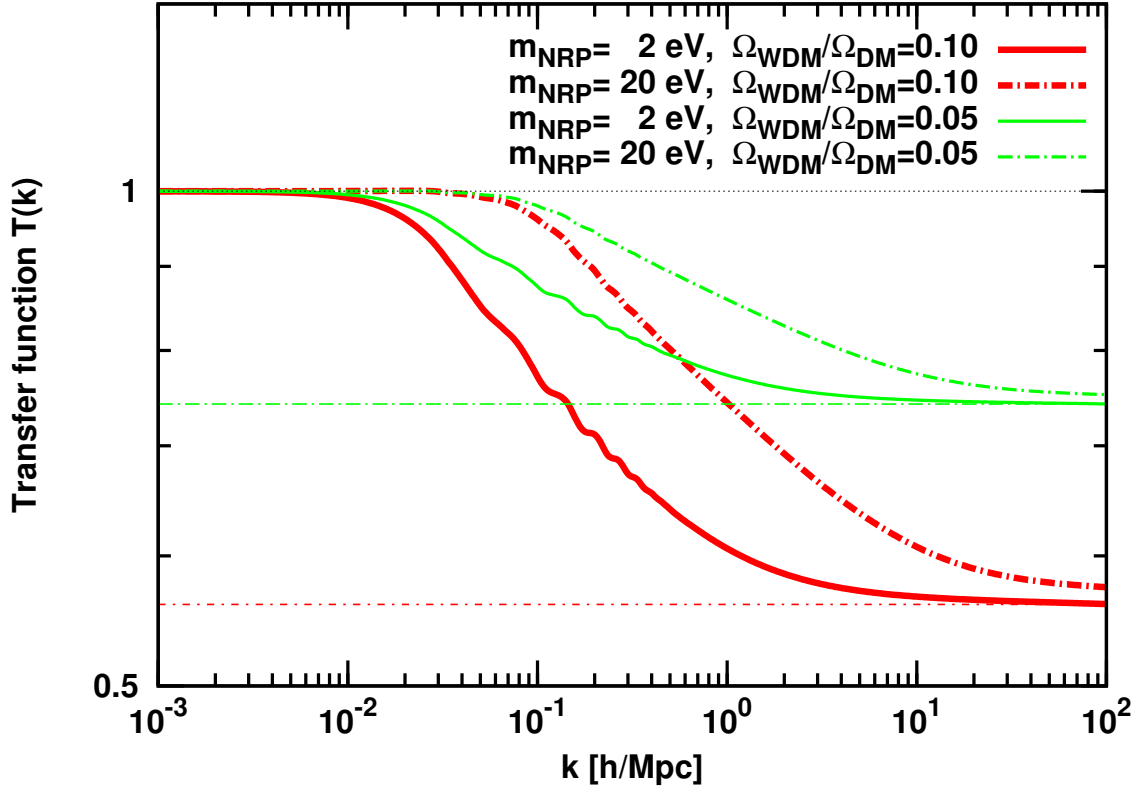
Figure 2. The height of plateau in the transfer function $T(k) \equiv [P_{\Lambda\text{CWDM}}(k)/P_{\Lambda\text{CDM}}(k)]^{1/2}$ depends only on f_{WDM} only and does not change with the mass. In these examples, the mass is equal to 2 eV (solid line) or 20 eV (dashed-dotted line), while $\Omega_{\text{WDM}}/(\Omega_{\text{WDM}} + \Omega_{\text{CDM}}) = 0.1$ (red) or 0.05 (green). Other parameters are fixed to $\Omega_{\text{B}} = 0.05$, $\Omega_{\text{M}} = 0.3$, $\Omega_{\Lambda} = 0.7$, $h = 0.7$.

This scale can be computed easily if we neglect the impact of Λ (it is easy to check that the contribution of the Λ-dominated stage to the above integral is completely negligible; actually, neglecting also the matter-dominated stage would be sufficient for an order of magnitude estimate). We can decompose the integral as:

$$\lambda_{\text{FSH}}^0 = \int_0^{a_{\text{nr}}} \frac{da}{a^2 H} + \frac{3T_\nu^0}{m_{\text{NRP}}} \int_{a_{\text{nr}}}^1 \frac{da}{a^3 H} \qquad (2.9)$$

with $a_{\text{nr}} = T_\nu^0/m_{\text{NRP}}$ being the scale factor at the time of the non-relativistic transition. Using the Friedman equation, this becomes

$$\lambda_{\text{FSH}} = \frac{1}{\sqrt{\Omega_R}H_0} \int_0^{a_{\text{nr}}} da + \frac{3a_{\text{nr}}}{\sqrt{\Omega_R}H_0} \int_{a_{\text{nr}}}^1 \frac{da}{a\sqrt{1 + a_{\text{eq}}/a}} \qquad (2.10)$$

where $a_{\text{eq}} = \Omega_R/\Omega_M$ is the scale factor at the time of matter/radiation equality. In the limit $a_{\text{nr}} \ll 1$, the result is simply

$$\lambda_{\text{FSH}}^0 = \frac{a_{\text{nr}}}{\sqrt{\Omega_R}H_0} \left(1 + 6\,\text{Arcsinh}\sqrt{\frac{a_{\text{eq}}}{a_{\text{nr}}}} \right) \simeq \frac{a_{\text{nr}}}{\sqrt{\Omega_R}H_0} \left(1 + 3\ln\left[4\frac{a_{\text{eq}}}{a_{\text{nr}}}\right] \right) \qquad (2.11)$$

which corresponds to the wavenumber

$$k_{\text{FSH}}^0 = \sqrt{\Omega_R} H_0 \frac{m_{\text{NRP}}}{T_\nu^0} \left(1 + 3 \ln \left[4 \frac{\Omega_R}{\Omega_M} \frac{m_{\text{NRP}}}{T_\nu^0} \right] \right)^{-1} \tag{2.12}$$

Taking $\Omega_R h^2 = 4 \times 10^{-5}$ we finally obtain

$$k_{\text{FSH}}^0 = 0.5 \left(\frac{m_{\text{NRP}}}{1 \text{ keV}} \right) \left(\frac{0.7}{h} \right) \left(1 + 0.085 \ln \left[\left(\frac{0.1}{\Omega_M h^2} \right) \left(\frac{m_{\text{NRP}}}{1 \text{ keV}} \right) \right] \right)^{-1} h/\text{Mpc} . \tag{2.13}$$

One can check in figure 2 that this corresponds indeed to the scale at which the ΛCWDM power spectrum starts to differ from the ΛCDM one. Note that the distinction between the free-streaming horizon and the free-streaming scale is not commonly used, because in the case of active neutrinos (which become non-relativistic during matter domination) one has $k_{\text{FSH}}^0 \sim k_{\text{FS}}^{\min}$; in this case, it is not necessary to introduce the quantity k_{FSH}, and the scale marking the beginning of the step is usually said to be $k_{\text{FS}}^{\min} = k_{\text{FS}}^{\text{nr}}$. In the case of WDM or CWDM, the distinction is important, because between t_{nr} and t_{eq} the free-streaming scale λ_{FS} remains constant, while the free-streaming horizon λ_{FSH} increases typically by one order of magnitude.

2.2 Plateau in CWDM

We can try to estimate the amplitude T_{plateau} of the small-scale power spectrum suppression,

$$T_{\text{plateau}} \equiv \left[\frac{P_{\Lambda\text{CWDM}}(k)}{P_{\Lambda\text{CDM}}(k)} \right]^{1/2} \qquad \text{for} \qquad k \gg k_{\text{FS}}^0 = 8 \times 10^2 \left(\frac{m_{\text{NRP}}}{1 \text{ keV}} \right) h/\text{Mpc} . \tag{2.14}$$

Let us consider a ΛCDM and a ΛCWDM model sharing the same cosmological parameters, and in particular the same Ω_{DM} and Ω_{B}. For simplicity, we neglect the mass of active neutrinos throughout this work. Until the time at which the warm component of the ΛCWDM model becomes non-relativistic, these models are indistinguishable. After this transition, but still before matter/radiation equality, the evolution of the gravitational potential is fixed by that of the photon and neutrino components, which dominate over dark matter; hence, the (slow) growth of cold dark matter inhomogeneities, $\delta_{\text{CDM}} \equiv \delta\rho_{\text{CDM}}/\rho_{\text{CDM}}$, is independent of f_{WDM}. We conclude that for any wavenumber k, $\delta_{\text{CDM}}(a_{\text{eq}})$ is the same in the two cases $f_{\text{WDM}} = 0$ and $f_{\text{WDM}} \neq 0$.

After equality, the evolution of the gravitational potential is fixed by the clustering of the dark matter and baryon components. Inside the Hubble radius, the growth of δ_{CDM} can be inferred from the Newtonian equation of evolution

$$\ddot{\delta}_{\text{CDM}} + \frac{\dot{a}}{a} \dot{\delta}_{\text{CDM}} = 4\pi \mathcal{G} a^2 \delta\rho_{\text{TOT}} = \frac{3}{2} \left(\frac{\dot{a}}{a} \right)^2 \frac{(\rho_{\text{CDM}} + \rho_{\text{B}})\delta_{\text{CDM}} + \rho_{\text{WDM}}\delta_{\text{WDM}}}{\rho_{\text{TOT}}} \tag{2.15}$$

where we used the fact that $\delta_{\text{CDM}} = \delta_{\text{B}}$ soon after equality, and a dot denotes a derivative with respect to conformal time. In the ΛCDM model (with $\rho_{\text{WDM}} = 0$), this equation has a well-known solution leading today to

$$\delta_{\text{CDM}}(a_0) = \left(\frac{a_0 g(a_0)}{a_{\text{eq}}} \right) \delta_{\text{CDM}}(a_{\text{eq}}) \tag{2.16}$$

where the constant $g(a_0) \leq 1$ is determined by the value of $\Omega_\Lambda = 1 - \Omega_{\text{M}}$, and describes the reduction in the perturbation growth rate during the Λ dominated epoch. It is roughly approximated by

$$g(a_0) \simeq \Omega_{\text{M}}^{0.2} \left(1 + 0.003(\Omega_\Lambda/\Omega_{\text{M}})^{4/3} \right) . \tag{2.17}$$

(see e.g. [94] for details). A more precise numerical evaluation gives $g(a_0) = 0.779$ for $\Omega_\Lambda = 0.7$. The product $a\,g(a)$ is usually called the linear growth factor.

In the ΛCWDM model, ρ_{WDM} cannot be neglected in the term ρ_{TOT} appearing in equation (2.15), but the warm component never clusters on small scales with $k > k_{\mathrm{FS}}^0$, so that δ_{WDM} can be set to zero. Then, a factor

$$\frac{\rho_{\mathrm{CDM}} + \rho_{\mathrm{B}}}{\rho_{\mathrm{TOT}}} \tag{2.18}$$

appears in the right hand-side of equation (2.15). During matter domination, this factor is equal to $(1 - f_{\mathrm{WDM}})$ and the linear growth factor can be found exactly (like in the case of ΛCHDM models with massive active neutrinos):

$$\delta_{\mathrm{CDM}}(a) = \left(\frac{a}{a_{\mathrm{eq}}}\right)^{1-(3/5)f_{\mathrm{WDM}}} \delta_{\mathrm{CDM}}(a_{\mathrm{eq}}) . \tag{2.19}$$

During Λ domination, there is no simple analytic result. In the case of ΛCHDM, it has been shown in ref. [94] that a very good approximation is found by just inserting the function $g(a)$ inside the parenthesis. In our case, the same ansatz would give

$$\delta_{\mathrm{CDM}}(a_0) = \left(\frac{a_0 g(a_0)}{a_{\mathrm{eq}}}\right)^{1-(3/5)f_{\mathrm{WDM}}} \delta_{\mathrm{CDM}}(a_{\mathrm{eq}}) \tag{2.20}$$

leading to a reduction in clustering with respect to the ΛCDM model equal to

$$\frac{\delta_{\mathrm{CDM}}^{f_{\mathrm{WDM}}}(a_0)}{\delta_{\mathrm{CDM}}^{f_{\mathrm{WDM}}=0}(a_0)} = \left(\frac{a_0 g(a_0)}{a_{\mathrm{eq}}}\right)^{-(3/5)f_{\mathrm{WDM}}} . \tag{2.21}$$

The power spectrum $P(k)$ is defined as the variance of the total matter perturbation

$$\frac{\delta\rho}{\rho} = \frac{\rho_{\mathrm{B}}\delta_{\mathrm{B}} + \rho_{\mathrm{CDM}}\delta_{\mathrm{CDM}} + \rho_{\mathrm{WDM}}\delta_{\mathrm{WDM}}}{\rho_{\mathrm{B}} + \rho_{\mathrm{CDM}} + \rho_{\mathrm{WDM}}} . \tag{2.22}$$

Today, $\delta_{\mathrm{B}} = \delta_{\mathrm{CDM}}$, and in the ΛCWDM model $\delta_{\mathrm{WDM}} \ll \delta_{\mathrm{CDM}}$ for $k > k_{\mathrm{FS}}^0$. So, on such small scales, on has

$$P_{\Lambda\mathrm{CDM}}(k) = \langle \delta_{\mathrm{CDM}}^2 \rangle , \qquad P_{\Lambda\mathrm{CWDM}}(k) = (1 - f_{\mathrm{WDM}})^2 \langle \delta_{\mathrm{CDM}}^2 \rangle . \tag{2.23}$$

Using equations (2.21) and (2.23), the suppression factor defined in eq. (2.14) is found to be:

$$T_{\mathrm{plateau}} = (1 - f_{\mathrm{WDM}}) \left(\frac{a_0 g(a_0)}{a_{\mathrm{eq}}}\right)^{-(3/5)f_{\mathrm{WDM}}} . \tag{2.24}$$

This equation is slightly different from the equivalent result in ΛCWDM models, due to the fact that the WDM component becomes non-relativistic during radiation domination.

Equation (2.24) encodes the right dependence of T_{plateau} on f_{WDM}, but cannot fit accurately the numerical results of a Boltzmann code for two reasons:

– first, in the above solution, we treated the transition from radiation to matter domination as an instantaneous process. In fact, matter comes to dominate in a progressive way, and $\delta_{\mathrm{CDM}}^{f_{\mathrm{WDM}}}(a)$ starts to depart from $\delta_{\mathrm{CDM}}^{f_{\mathrm{WDM}}=0}(a)$ slightly *before* the time of equality.

Hence, the ratio $\delta_{\rm CDM}^{f_{\rm WDM}}(a_{\rm eq})/\delta_{\rm CDM}^{f_{\rm WDM}=0}(a_{\rm eq})$ is actually smaller than one and decreases when $f_{\rm WDM}$ increases. This means that equation (2.24) slightly underestimates the effect of WDM. Empirically, we found that this can be corrected by increasing the exponential factor from 3/5 to 3/4 (at least, as long as $\Omega_{\rm M}$ does not depart too much from 0.3). In figure 3, we compare the result of a full Boltzmann code calculation (using CAMB [95]) with the empirical fit

$$T_{\rm plateau} = (1 - f_{\rm WDM}) \left(\frac{a_0 g(a_0)}{a_{\rm eq}} \right)^{-(3/4) f_{\rm WDM}} \tag{2.25}$$

and find very good agreement. In this example,

$$\alpha \equiv \frac{a_0 g(a_0)}{a_{\rm eq}} = \frac{\Omega_{\rm M}}{\Omega_{\rm R}} g(a_0) = \frac{\Omega_{\rm M} h^2 g(a_0)}{4.16 \times 10^{-5}} = 2.75 \times 10^3 \tag{2.26}$$

for $T_{\rm CMB} = 2.726$ K, $\Omega_\Lambda = 0.7$, $\Omega_{\rm M} = 0.3$, $h = 0.7$.

– second, we assumed that in all cases one has $\delta_{\rm B} \simeq \delta_{\rm CDM}$ soon after equality. However, we are interested here in very small scales ($k \sim 100h/{\rm Mpc}$) for which the baryon and CDM overdensities do not converge towards each other before the end of matter domination. Hence, the approximations $\delta_{\rm CDM} \propto a$ or $\delta_{\rm CDM} \propto a^{1-(3/5)f_{\rm WDM}}$ only apply to a short period: at the beginning of matter domination, baryons do not contribute to the right-hand side of equation (2.15), and the growth of $\delta_{\rm CDM}$ is slower. Since this effect (governed by the parameter $\Omega_{\rm B}/\Omega_{\rm M}$) is similar in the two cases $f_{\rm WDM} \neq 0$ and $f_{\rm WDM} = 0$, one does not expect a strong dependence of $T_{\rm plateau}$ on the baryon abundance. As can be seen in figure 3, the Boltzmann code calculation shows that even radical variations in $\Omega_{\rm B}$ hardly affect the behavior of the suppression factor. We conclude that equation (2.25) is accurate up to a few percent for realistic ΛCWDM models.[4]

For small $f_{\rm WDM}$, one can expand equation (2.25) to obtain:

$$T_{\rm plateau}^2 \approx 1 - 2f_{\rm WDM} - \frac{6}{4} f_{\rm WDM} \log \alpha \approx 1 - 14 f_{\rm WDM} . \tag{2.27}$$

This expression can be compared with $T_{\rm plateau}^2 \approx 1 - 8f_\nu$ obtained in the case of active neutrinos [96].

Note that equation (2.25) applies today, but the suppression factor at higher redshift can simply be obtain by replacing a_0 by $a = a_0/(1 + z)$; so, it is clear that the transfer function $T(k)$ is redshift-dependent, with a smaller step-like suppression at large z. The function $T(k)$ is only expected to vary with z on scales such that $\delta_{\rm WDM}(z) < \delta_{\rm CDM}(z)$, i.e. for $k > k_{\rm FS}(z)$. This redshift dependence is illustrated in figure 4.

3 Ly-α method

In order to constrain cosmological models, it is always preferable to rely on data dealing with linear scales. However, we have seen in the previous section that the difference between ΛCDM and ΛCWDM (or ΛWDM) models appears only on small scales (typically, $k >$

---

[4]This statement is meant for the plateau scales $k \sim 100h/{\rm Mpc}$. At much larger k, the situation becomes more complicated, since according to the linear theory one has $\delta_{\rm B} < \delta_{\rm CDM}$ even today.
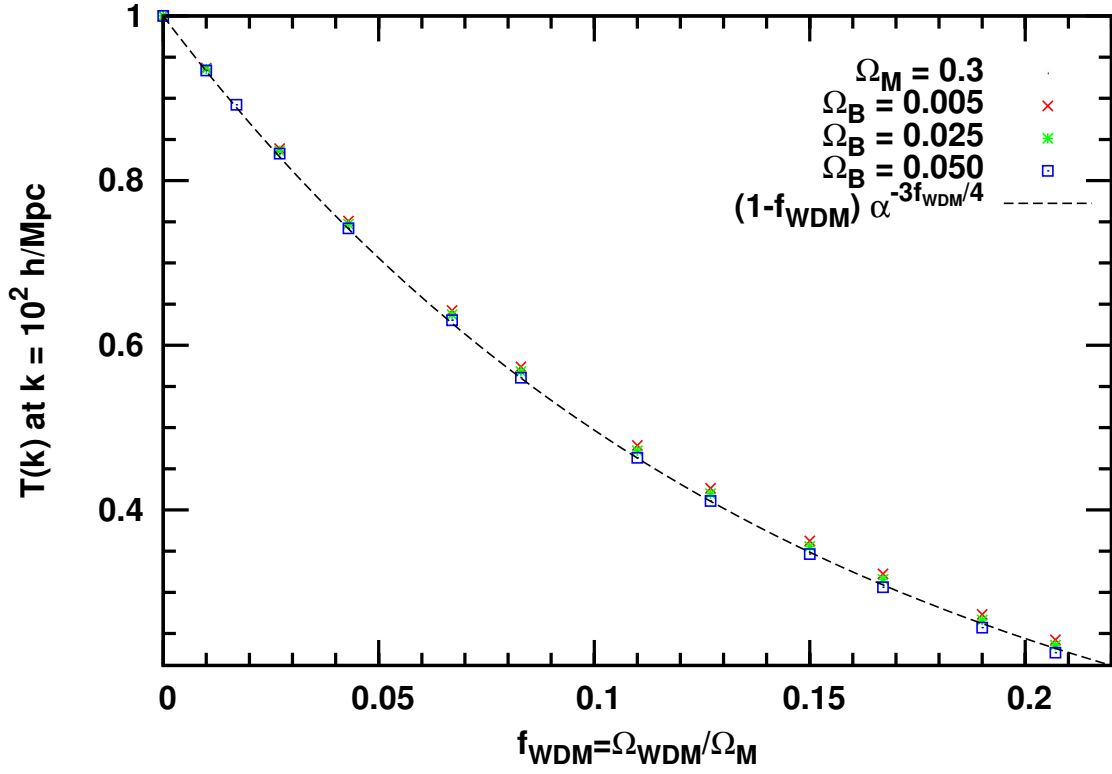
Figure 3. Suppression factor $T_{\text{plateau}} = [P_{\Lambda\text{CWDM}}(k)/P_{\Lambda\text{CDM}}(k)]^{1/2}$ computed today at $k = 10^2\,h/\text{Mpc}$ with the Boltzmann code CAMB, for different values of $f_{\text{WDM}} \equiv \Omega_{\text{WDM}}/\Omega_{\text{M}}$ and Ω_{B}. Other parameters are kept fixed: $\Omega_\Lambda = 0.7$, $\Omega_{\text{M}} = 0.3$, $h = 0.7$. The dashed curve corresponds to the analytic prediction of eq. (2.25) with $\alpha \equiv a_0 g(a_0)/a_{\text{eq}} = 2.75 \times 10^3$.
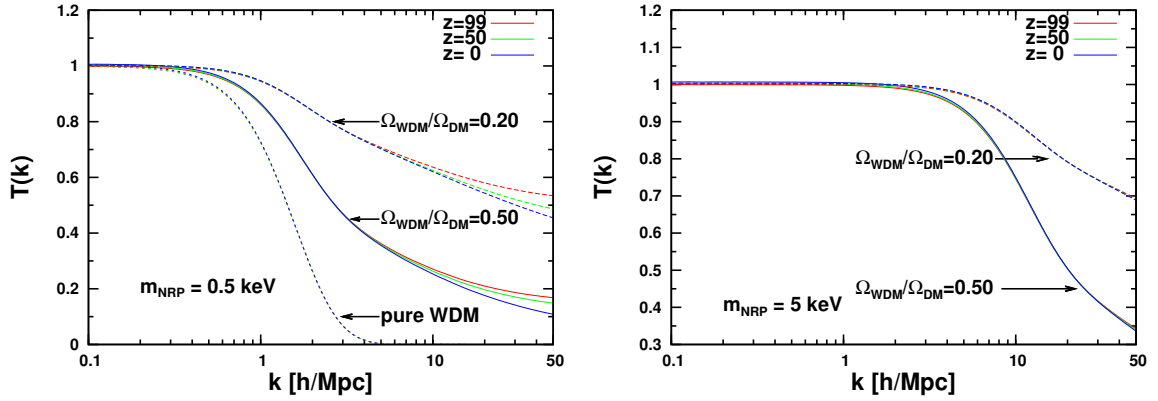
Figure 4. Variation of $T(k) = [P_{\Lambda\text{CWDM}}(k)/P_{\Lambda\text{CDM}}(k)]^{1/2}$ with redshift, for various values of m and $\Omega_{\text{WDM}}/(\Omega_{\text{WDM}} + \Omega_{\text{CDM}})$; other parameters are fixed to the same values as in previous figures. *(Left)* For $m = 0.5$ keV, the variation is clearly visible at large $k > k_{\text{FS}}(z)$. *(Right)* For $m = 5$ keV, the free-streaming wavenumber is too large for any variation to be seen on the scales displayed here.

0.1 h/Mpc) which cannot be probed by CMB experiments, or by the reconstruction of the galaxy power spectrum in the range in which the light-to-mass bias can be treated as scale-

independent. Hence, at the moment, the only way to discriminate between ΛCDM and ΛCWDM (or ΛWDM) models is to use observations of Lyman-α (Ly-α) absorption in the spectrum of distant quasars (QSOs), which can be used as a tracer of cosmological fluctuations on scales $k \sim (0.1-10)\,h\,\text{Mpc}^{-1}$, at redshifts $z \sim (2-4)$ where the cosmological perturbations are already affected by the non-linear evolution — although not as much as today.

The Ly-α forest is a dense set of absorption lines observed in QSO spectra. It is well established by analytical calculations and hydrodynamical simulations that these absorption lines correspond to Ly-α absorption ($1s \rightarrow 2p$) by clouds of neutral hydrogen at different redshifts along the line of sight. This neutral hydrogen is part of the warm ($\sim 10^4$ K) and photoionized intergalactic medium (IGM). Opacity fluctuations in the spectra arise from fluctuations in the neutral hydrogen density, from which it is possible to infer fluctuations in the total matter distribution [97–99]. For each quasar, the observed spectrum $I(z)$ can be expanded in (one-dimensional) Fourier space. The expectation value of the squared Fourier spectrum is called the *flux power spectrum*. The data provide an estimate of the flux power spectrum P_F for various redshifts $z \sim 2-4$ (for which light rays of wavelength $\lambda_{\text{obs}} = (1+z)1265\mathring{A}$ pass through the optical window of the Earth's atmosphere). At these redshifts, the density perturbations of scales $k \sim (0.1-10)\,h\,\text{Mpc}^{-1}$ already entered into a mildly non-linear stage of gravitational collapse ($\delta\rho/\rho \gtrsim 1$).

The linear matter power spectrum $P(k)$ and the flux power spectrum $P_F(k)$ are complicated functions of the cosmological parameters. In the rather narrow range of scales probed by Ly-α data, the effects of an admixture of WDM might be compensated by a change in other cosmological parameters (σ_8, $\Omega_M h^2$, n_s, etc.), or even in extra astrophysical parameters in the case of the flux power spectrum. Therefore, it is important to perform collective fits to the Ly-α data and other data sets (e.g. CMB). Cosmological parameter extraction from combined cosmological data sets can be conveniently performed with a Monte-Carlo Markov Chain (MCMC) technique, using e.g. the public code COSMOMC [100]).

In order to predict $P_F(k,z)$ for a given cosmological model, it is necessary to perform hydrodynamical simulations (while for CMB experiments probing the linear matter power spectrum, it is sufficient to compute the evolution of linear cosmological perturbations using a Boltzmann code like CAMB). Hydrodynamical simulations are necessary both for simulating the non-linear stage of structure formation and for computing the evolution of thermodynamical quantities (in order to relate the non-linear matter power spectrum to the observable flux power spectrum). The characteristic number of samples required for a reliable determination of parameter probabilities ranges from 10^3 for the simplest cosmological scenario to 10^4 (or even 10^5) when more parameters and freedom are introduced in the model. In principle, in order to fit Lyman-α data, one should perform a full hydrodynamical simulation for each Monte-Carlo sample. This is computationally prohibitive, and various simplifying approximations have been proposed [50, 60–63, 101–103]. Below, we discuss the two datasets used in this paper, for which different strategies have been implemented.

3.1 VHS data

The VHS dataset was compiled in ref. [91] using 57 QSO spectra from LUQAS [104] at $z \sim 2.1$, and from ref. [105] at $z \sim 2.7$. Each spectrum was observed with high resolution and high signal-to-noise, resulting in clean and robust measurements. However, this dataset is based on a relatively small number of spectra, leading to a large statistical uncertainty. Systematic errors were estimated in a conservative way, and the flux power spectrum was only used in the range 0.003 s/km $< k <$ 0.03 s/km (roughly corresponding to scales 0.3 h/Mpc $<$

$k < 3$ h/Mpc): at larger scales, the errors due to uncertainties in fitting a continuum (i.e. in removing the long wavelength dependence of the spectrum emitted by each QSO) become very large, while at smaller scales, the contribution of metal absorption systems becomes dominant. It was shown in ref. [91] that the dependence of the bias function $b(k, z) \equiv P_F(k, z)/P(k, z)$ on cosmological parameters can be neglected for this data set, given the large systematic plus statistical errorbars in VHS, and the limited range in k-space and z-space probed by this data [50]. Hence, this bias function can be computed for a fiducial model, and the data points $P_F(k_i, z_j)$ can be translated in linear spectrum measurements $P(k_i, z_j)$. This approach is implemented in the public module `lya.f90` [63] distributed with COSMOMC. We will use this dataset in section 5 to derive conservative estimates.

3.2 SDSS data

For the Ly-α data obtained by the SDSS collaboration [92], a different approach has been implemented in ref. [61]. The data points were obtained from 3035 quasar spectra with low resolution and low signal-to-noise, spanning a wide range of redshifts ($z = 2.2 - 4.2$). Dealing with low resolution and low signal-to-noise QSO spectra and extracting the flux power is a very difficult task as shown in [61]. We refer to their analysis for a comprehensive study of continuum fluctuations removal, metal lines contamination, presence of damped Ly-α systems, resolution of the spectrograph and noise level in each redshift bins. All these effects need to be properly taken into account, and not modelling them properly would impact the obtained flux power in a way that is difficult to predict. In the following, we will use the flux power provided by the SDSS collaboration, introducing nuisance parameters for the resolution and noise in each redshift bin as suggest by [61, 92], and implicitly assuming that all the contaminants above have been either removed or properly modelled in their analysis.

The low resolution of SDSS data implies that the flux power spectrum cannot be measured on small scales (with $k \geq 0.02$ s/km). However, on larger scales, the low resolution and signal-to-noise are compensated by the statistics: with such a large number of quasars, statistical errorbars on the flux power spectrum are much smaller than for VHS data. Hence, using a fixed bias function would be inappropriate. Instead, ref. [61, 92] used a large number of fast hydro-particle-mesh (HPM) simulations [102, 106] densely sampling the cosmological parameter space, calibrated from a small number of full hydrodynamical simulations. These HPM runs could produce an inaccurate flux spectrum estimation for cosmological models departing from the fiducial points where the hydrodynamical simulations were performed, and a more reliable calibration is probably needed.

A different approximation scheme was used in ref. [62] using the same data. For each wavenumber and redshift, the flux power $P_F(k, z)$ was Taylor-expanded around a fiducial model at first order in cosmological parameters, using of the order of N full hydrodynamical simulations (here $N \sim 20$ is the number of relevant cosmological/astrophysical parameters). This method can also become inaccurate far from the fiducial model, especially when the likelihood and/or parameter posterior probability deviates significantly from a multivariate Gaussian distribution. However, in both methods, it can be checked a posteriori that the inaccuracy introduced by interpolating/extrapolating around the points where hydrodynamical simulations were performed is negligible with respect to data error bars, at least in the range of cosmological models producing reasonable fits to the data.

We deal with uncertainties related to Ly-α physics in the same way as in ref. [61, 62]. Namely, we use 9 "astrophysical" nuisance parameters. Two describe the effective evolution of the optical depth, six describe the evolution of the parameters γ and T_0 entering the relation

between the temperature of the intergalactic medium and its overdensity, $T = T_0(1 + \delta)^{\gamma-1}$. The parameter T_0 was allowed to vary in the range $0 \leq T_0 \leq 10^5$ K, while $0 \leq \gamma \leq 2$. Note that the range of parameters chosen is very wide and embraces also the recent results of [55] that found evidences of an inverted ($\gamma < 1$) temperature-density relation. The parameters describing the thermal evolution are modelled as a broken power-law at $z = 3$ as $y = A \left(\frac{1+z}{4}\right)^S$, with one parameter for the amplitude and two for the slopes at $z < 3$ and $z > 3$ (the slopes are left free to vary in the range $[-6, 6]$). This is done in order to better mimic more complex evolutions able for example to reproduce the Helium II reionization at $z \sim 3$ as suggested by SDSS observations [107]. The evolution of the effective optical depth is modeled as a single power-law (two parameters: one for the amplitude and one for the slope) within a very wide observational range. Another parameter describes the contribution of strong absorption systems (Damped Lyman-α systems) and this is left free following exactly the suggestions of ref. [61] and applying the correction of ref. [108].

Finally, we have a total of 9 additional parameters that model uncertainties in the correction to the data — eight parameters for the noise correction in various redshift bins, and one parameter describing the error of the resolution correction (these parameters do have strong a-posteriori priors as in ref. [61]). All these parameters as well as those describing corrections for damped/high column density systems are constrained as suggested in [108] and described in [62].

When deriving bounds on the parameters of interest below, we marginalized over these 18 parameters, and the final estimates of the astrophysical parameters are within the observational bounds.

In order to take into account the contribution of SiIII metal lines to the power spectrum, we followed an approach similar to the one suggested in [61]. Namely, we introduced an extra parameter, describing the contribution of SiIII lines to the power spectrum, and fixed it to the maximum correction suggested by the SDSS collaboration [61], motivated by the following arguments: i) the metal lines contribution peaks at smaller scales than those investigated here; ii) at large scales the effect is an overall suppression of power which is already taken into account by the fact that we are considering a wide range of possible mean effective optical depths ([104]); iii) the effect of modelling further the SiIII metal contribution by allowing z-dependence has been found to have a small impact on the final results by ref. [61].

Within the range allowed by the data, the effect of ΛCDM cosmological parameters and astrophysical parameters on the flux power spectrum is nearly linear, as can be checked *a posteriori* from the fact that all marginalized probabilities are almost Gaussian. This justifies the use of a first-order Taylor expansion. The authors of ref. [62] checked this explicitly for some parameters, by performing a second order Taylor expansion or by trying to estimate the flux power in regions of the parameter space that are very far from the best-fit with a full hydrodynamical simulation. They usually found good agreement between the various methods at the percent level in the simulated flux power.

In the present work, we want to obtain constraints on mixed ΛCWDM models. The parameter probability distribution is strongly non-Gaussian with respect to the extra parameters characterizing this set-up: the density fraction of warm dark matter, and its mass (or velocity dispersion). Hence, a simple first-order Taylor expansion would lead to inaccurate results. In section 6, we extend the method of [62] by interpolating between a grid of fiducial models in this two-dimensional sub-space, while keeping a simple Taylor expansion in other parameters. To this end, we performed a grid of 8 additional simulations (for two values of the masses and four values of the warm dark matter fraction). In the next section, we will

discuss the robustness of these simulations, especially as far as the issue of initial velocities is concerned.

4 Thermal velocities in ICs

In N-body or hydrodynamical simulations, the difference between Initial Conditions (ICs) for CDM and WDM does not reside entirely in a modification of the power spectrum, but also in non-negligible thermal velocities for the warm component. For Thermal Relics (TR) assumed to decouple from thermal equilibrium when they are still relativistic, and characterized by a Fermi-Dirac distribution with temperature T_{TR}, the average velocity is given by

$$\langle v_{\text{TR}} \rangle = \frac{3.151 \, T_{\text{TR}}(z)}{m_{\text{TR}}} = \left(\frac{1+z}{100} \right) \left(\frac{1 \text{ keV}}{m_{\text{TR}}} \right) \left(\frac{T_{\text{TR}}}{1 \text{ K}} \right) 8.07 \text{ km.s}^{-1}. \tag{4.1}$$

However, in this paper, we assume that WDM consists in sterile neutrinos produced through a Non-Resonant Production (NRP) mechanism, namely, non-resonant oscillations with active neutrinos [15, 80, 82]. In this case the distribution can be roughly approximated by the renormalized Fermi-Dirac distribution of eq. (2.1), corresponding to an average velocity

$$\langle v_{\text{NRP}} \rangle = \frac{3.151 T_\nu(z)}{m_{\text{NRP}}} = \frac{3.151 (4/11)^{1/3} (1+z) T_{\text{CMB}}}{m_{\text{NRP}}} = \left(\frac{1+z}{100} \right) \left(\frac{1 \text{ keV}}{m_{\text{NRP}}} \right) 15.7 \text{ km.s}^{-1}. \tag{4.2}$$

If the mass and the relic density $\Omega_{\text{WDM}} h^2$ are specified, the parameter T_{TR} (for TR) or χ (for NRP) can be inferred from $(T_{\text{TR}}/T_\nu)^3 = \chi = \Omega_{\text{WDM}} h^2 (94 \text{ eV}/m)$. Thermal relics and sterile neutrinos sharing the same mass and density correspond to different initial velocities. For instance, assuming that $\Omega_{\text{WDM}} h^2 = 0.12$, we find the following velocity dispersion at $z = 99$ in each of the two cases:

$$
\begin{array}{lll}
m = 10 \text{ keV} & \langle v_{\text{NRP}} \rangle \approx 1.6 \text{ km/sec} & \langle v_{\text{TR}} \rangle \approx 0.16 \text{ km/sec} \\
m = 5 \text{ keV} & \langle v_{\text{NRP}} \rangle \approx 3.1 \text{ km/sec} & \langle v_{\text{TR}} \rangle \approx 0.41 \text{ km/sec} \\
m = 0.5 \text{ keV} & \langle v_{\text{NRP}} \rangle \approx 31 \text{ km/sec} & \langle v_{\text{TR}} \rangle \approx 8.8 \text{ km/sec}
\end{array} \tag{4.3}
$$

These velocities should be compared with the peculiar velocities which particles acquire when clustering. In most codes, the latter are initialized using the so-called Zel'dovich prescription [109–111]: so, later, we will make the distinction between *thermal velocities* and *Zel'dovich velocities*. Whenever the thermal velocities are negligible with respect to the Zel'dovich ones, the final result is expected to be insensitive to the proper implementation of thermal velocities, which can then be omitted from ICs. In a typical simulation, the Zel'dovich velocities are of below or around 20 km/s at $z = 99$. Hence, for the NRP case, we roughly expect. Hence, for the NRP case, we roughly expect that thermal velocities are unimportant for $m \geq 5$ keV.

This can be checked explicitly. Our numerical simulations are performed with the GADGET-II code [112], extended in order to compute the Ly-α flux power spectrum [60]. First, we address the case of pure ΛWDM models with $\Omega_{\text{CDM}} = 0$. We fix initial conditions at $z = 99$. The initial power spectrum is computed with CAMB, and for each warm particle a random thermal velocity is eventually added to the Zel'dovich velocity. Thermal velocities are distributed with a Fermi-Dirac probability.

Notice, however, that a particle in the simulated ICs represents a region with size $l = L_{\text{box}}/N^{1/3}$ (where N is the number of particles) . Therefore, a huge amount of DM

particles are represented as one body in N-body simulations. Formally, the velocity of such a collection of particles is zero, as the velocities of real DM particles are random and they average to zero. The assignment of a Fermi-Dirac thermal velocity to such a simulation particle is justified provided that l is smaller than the smallest scale probed by our data set, and larger than the extra distance traveled by the particle, due to thermal velocities, when it moves along Zel'dovich trajectories. In our simulation, we take $N = 400^3 = 6.4 \times 10^7$ particles in a box of comoving size $L_{\mathrm{box}} = 60\,\mathrm{Mpc}/h$, so each resolution element in the ICs measures $l \sim 0.15\,\mathrm{Mpc}$ in comoving units, while the smallest scale probed by our Ly-α flux power spectrum corresponds to a comoving wavelength of the order of 1 Mpc. In addition, the extra distance travelled by the particle can be estimated conservatively by multiplying the velocity $v \sim 10\,\mathrm{km/s}$ by the amount of time between $z = 99$ and $z = 2$, $t \sim 3\,\mathrm{Gyr}$: this gives 0.04 Mpc, which is smaller than the resolution element probed by the particle in the ICs. Hence, our approach is justified. A similar way to include velocities in the WDM simulations was used e.g. in [113]. Note that the simulated flux power has been corrected for resolution using exactly the same procedure described in [66], so even if most of the simulations have been ran at somewhat low resolution we corrected for it using the higher resolution runs.

In figure 5, we show the ratio of the ΛWDM flux power spectrum to the ΛCDM one at $k = 0.14\,h/\mathrm{Mpc}$ and $z = 2.2$ for 3 masses ($0.5, 5, 10\,\mathrm{keV}$), with and without thermal velocities in ICs. One can see that for masses above $\sim 5\,\mathrm{keV}$, the influence of velocities is below the 1% level, which is smaller than the error bars of the SDSS data points (in case of the VHS dataset, the influence of velocities is unimportant also for smaller masses due to the larger error bars). For smaller masses, including thermal velocities in the initial conditions becomes essential.

This suggest that also in the case of a mixed ΛCWDM, we can perform simulations without thermal velocities provided that the mass of the WDM NRP component is above $\sim 5\,\mathrm{keV}$. This simplifies considerably the issue of initial conditions, because in this case we can treat the mixed CDM+WDM components as a single cold fluid with negligible thermal velocities, and a proper initial power spectrum (equal to the total linear matter power spectrum at high redshift, as computed by CAMB).

5 Results for VHS data

We performed a Bayesian parameter estimation for the ΛCWDM model, using the following data set: VHS Ly-α data; WMAP5 [114] and small-scale CMB experiments (ACBAR [115], CBI [116], Boomerang [117–120]); galaxy power spectrum from the SDSS LRGs [121]; supernovae from the SNLS [122]. We take flat priors on six cosmological parameters describing the ΛCDM model $(\Omega_{\mathrm{DM}}h^2, \Omega_{\mathrm{B}}h^2, \theta, \tau, n_s, A_s)$,[5] on two extra parameters describing the warm sector (see below), and we marginalize over nuisance parameters associated with the data sets, in the way implemented in the public version of CosMOMC (compiled with the file lya.f90). The two extra parameters are chosen to be:

- first, the warm fraction of dark matter,

$$F_{\mathrm{WDM}} \equiv \frac{\Omega_{\mathrm{WDM}}}{\Omega_{\mathrm{CDM}} + \Omega_{\mathrm{WDM}}}, \tag{5.1}$$

which differs from the quantity f_{WDM} defined in eq. (2.4) by $(\Omega_{\mathrm{DM}}/\Omega_M)$ since the denominator accounts for dark matter instead of total matter; indeed, in the analytical

---

[5]See e.g. [100] and http://cosmologist.info/cosmomc/readme.html for explanation of this parameter choice.
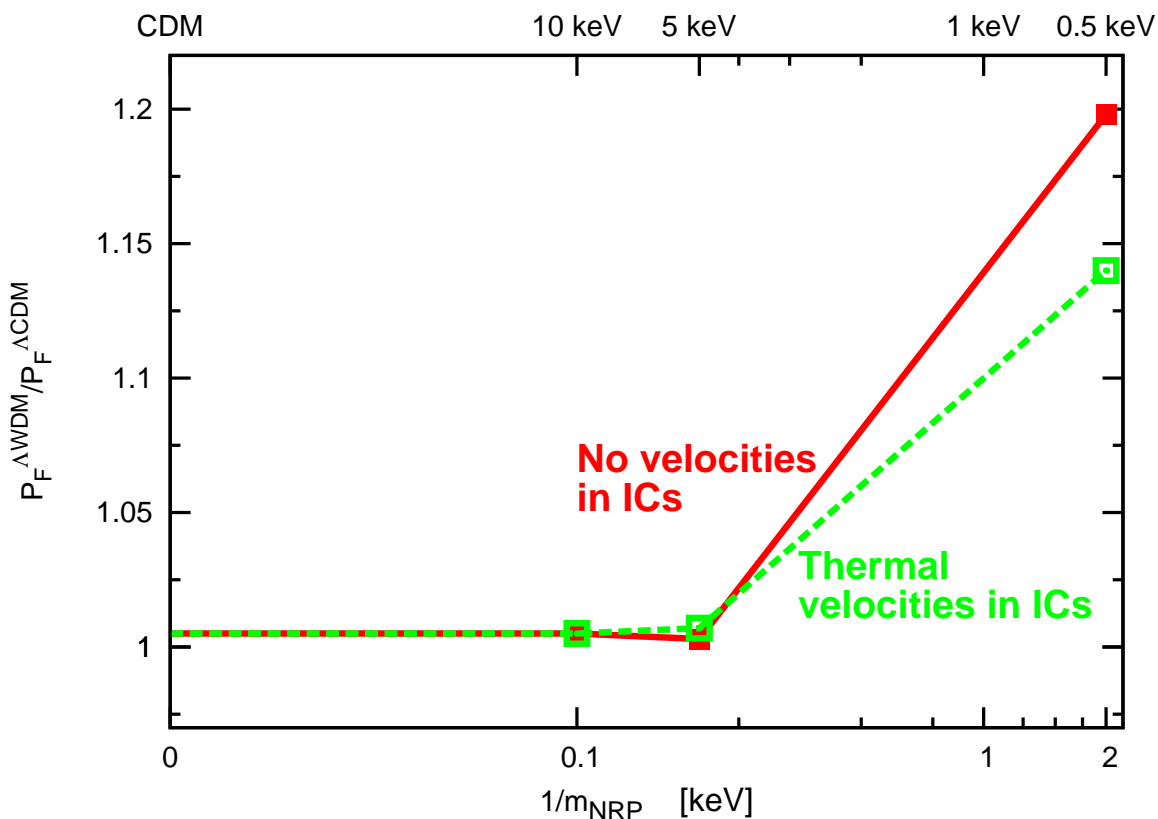
Figure 5. Dependence of the flux PS of ΛWDM models (divided by that of ΛCDM) on thermal velocities in hydrodynamical simulations. The points show $P_F^{\Lambda\mathrm{WDM}}/P_F^{\Lambda\mathrm{CDM}}$ at $k = 0.14\,h/\mathrm{Mpc}$ and $z = 2.2$, extracted from GADGET-II simulations for three different masses, with and without thermal velocities in the initial conditions. The lines are the results of linear interpolation between these points.

solutions of section 2, f_{WDM} is the quantity which appears naturally; in a parameter extraction, F_{WDM} is more convenient because of its clear interpretation: it varies from $F_{\mathrm{WDM}} = 0$ for pure cold to $F_{\mathrm{WDM}} = 1$ for pure warm dark matter. Instead, $f_{\mathrm{WDM}} = 1$ would describe a model with negligible CDM *and* baryonic components, providing very bad fits to the data, and an eventual upper limit on f_{WDM} would not be straightforward to interpret physically.

- the average velocity of warm particles today in km/s: $\langle v \rangle_{\mathrm{WDM}}$. This parameter is convenient because, unlike the particle mass, it has a direct physical effect on the power spectrum; hence our results apply to both NRP and TR models (and presumably to a much wider class of WDM models). Bounds on $\langle v \rangle_{\mathrm{WDM}}$ can be translated immediately in terms of m_{NRP} using eqs. (4.2); limits on m_{TR} are not so straightforward to obtain since they depends on the posterior distribution of $\langle v \rangle_{\mathrm{WDM}}$, F_{WDM} and Ω_{DM}.

Note that varying F_{WDM} and $\langle v \rangle_{\mathrm{WDM}}$ is equivalent to tuning respectively the size and the location of the step-like suppression in the matter power spectrum (at least at the linear level), as shown in section 2.

The main goal of the various MCMC runs performed in this work is to derive some
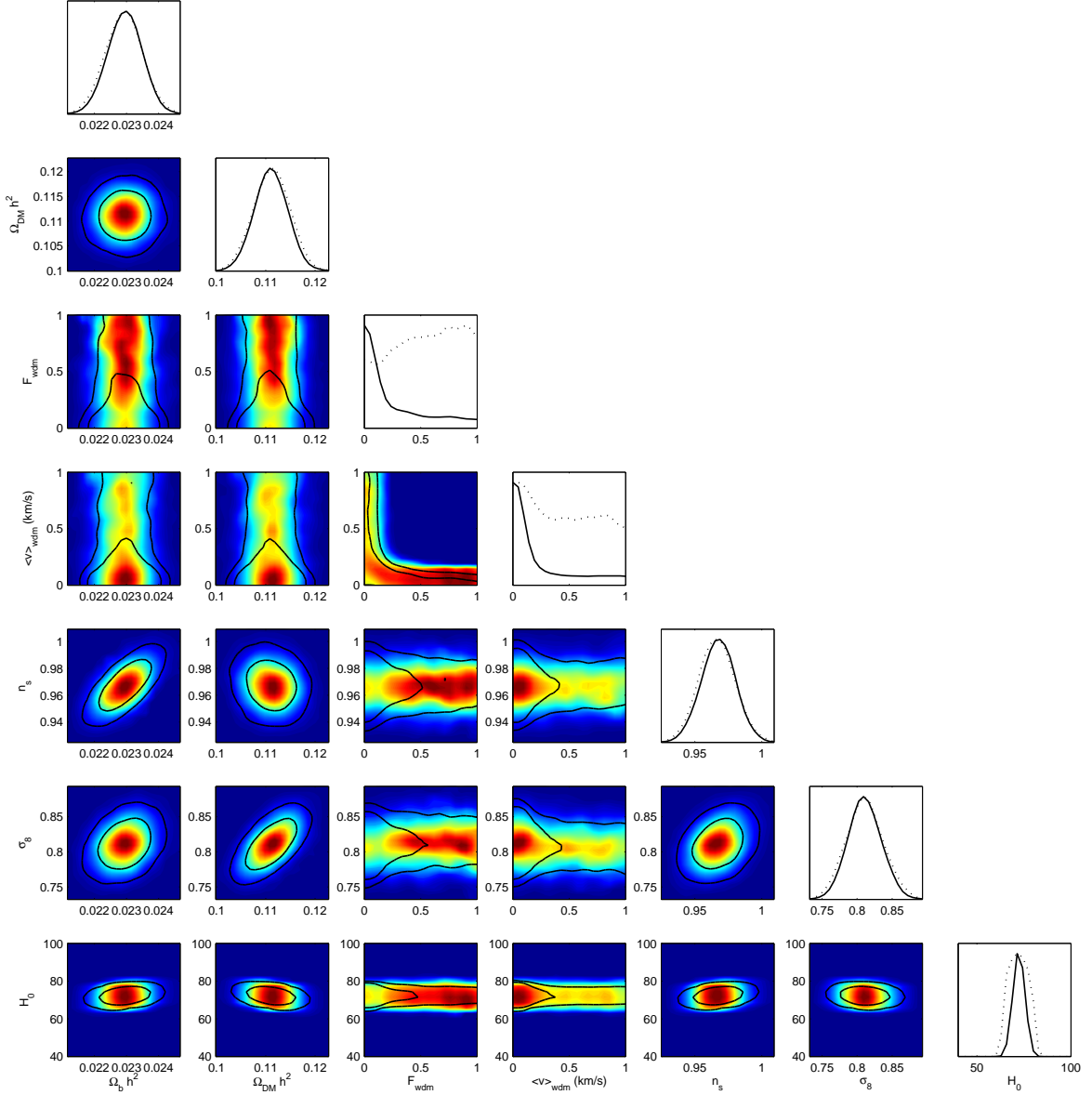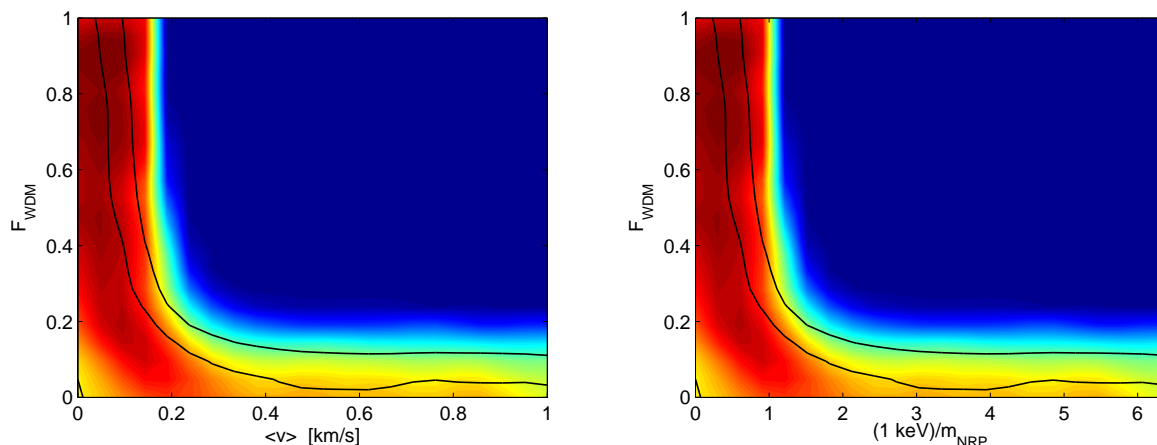
Figure 6. Preferred region for pairs of cosmological parameters in the ΛCWDM model, using VHS, WMAP5 and other cosmological data sets. The black lines represent the 68%CL and 95%CL contours of the two-dimensional probability marginalized over other parameters (as defined in the Bayesian approach), while the colors show the likelihood averaged over other parameters. The first five parameters $\Omega_{\rm B}h^2$, $\Omega_{\rm DM}h^2$, $F_{\rm WDM}$, $\langle v \rangle_{\rm WDM}$, n_s have flat priors over the displayed range. Our analysis also assumes flat priors on the logarithm of the primordial spectrum amplitude and on the angular diameter of the sound horizon, but instead of these parameters we show here σ_8 and H_0, which have a more straightforward interpretation. In this plot, we do not show the reionization optical depth τ and all the nuisance parameters entering into the analysis. The one-dimensional marginalized probabilities are displayed along the diagonal.

(Bayesian) credible intervals[6] for the parameter $\langle v \rangle_{\rm WDM}$, starting from a flat prior on this parameter in the range $0 < \langle v \rangle_{\rm WDM} < \infty$. These results can be immediately translated

---

[6]See the appendix A for a comparison of Bayesian *credible intervals* and frequentist *confidence limits*.

Figure 7. *(Left)* Preferred region for the parameters $(F_{\text{WDM}}, \langle v \rangle_{\text{WDM}})$ of the ΛCWDM model, using VHS, WMAP5 and other cosmological data sets. The black lines represent the 68%CL and 95%CL contours of the two-dimensional probability marginalized over other parameters (as defined in the Bayesian approach), while the colors show the likelihood averaged over other parameters. *(Right)* Same plot with the horizontal axis translated in terms of $(1\text{keV}/m_{\text{NRP}}) = \langle v \rangle_{\text{WDM}}/(157 \text{ m/s})$, see equation (4.2).

in credible intervals for m_{NRP}^{-1}, using the relation $(1 \text{ keV})/m_{\text{NRP}} = \langle v \rangle_{\text{WDM}}/(0.157 \text{ km/s})$, see equation (4.2) with $z = 0$. It would not be convenient to derive directly some credible intervals on m_{NRP} itself, since the ΛCDM limit (which is perfectly allowed by the data) corresponds to $m_{\text{NRP}} \longrightarrow \infty$. However, each 95% Confidence Level (CL) upper bound on $\langle v \rangle_{\text{WDM}}$ can be expressed as a lower bound on the mass, that we will denote as m_{NRP}^{95}. We warn the reader that this bound should be interpreted with care, since we are not using a flat prior on the mass, but rather on the velocity, i.e. on the inverse mass. Hence the quantity m_{NRP}^{95} represents a Bayesian 95% CL upper limit on the velocity expressed in a useful way.

We first ran CosmoMC with F_{WDM} fixed to one, in order to update bounds on the pure ΛWDM model. We found a credible interval $0 < \langle v \rangle_{\text{WDM}} < 0.10$ km/s (95% CL), which can be translated into the lower limit $m_{\text{NRP}}^{95} = 1.6$ keV. In reference [63] (which also used VHS Ly-α data, but WMAP1 instead of WMAP5), a stronger bound $m_{\text{NRP}}^{95} = 2.0$ keV was found. This is surprising at first sight, since the CMB temperature and polarization spectra are better measured by WMAP5. In addition, WMAP5 favors the lowest range of n_s and σ_8 values allowed by WMAP1, so one could expect that a cut-off in the power spectrum due to WDM is even more unlikely, leading to stronger bounds. Actually, the constraints on this cut-off come entirely from the VHS data: so, for ΛWDM models, the real expectation is that the mass bounds should remain almost insensitive to variations in the CMB data. Still, a possible explanation of this 20% discrepancy is that for ΛWDM (and ΛCWDM) models, the convergence of MCMCs requires a huge amount of samples. In this work, we deliberately accumulated a very large number of chain points, and checked thoroughly that our chains are fully converged.[7] The older result might have been affected by poorer chain convergence.

---

[7] This particular ΛWDM run is based on 6 independent chains. After accumulating a total of $\sim 30\,000$ chain points, we reached a convergence criterion $(R - 1) \sim 0.02$ (based on the second half of the full chains, see ref. [100] for a definition of R), and a bound $m_{\text{NRP}}^{95} = 2.0$ keV. However, it is only after accumulating $\sim 100\,000$ chain points that the bound stabilized to $m_{\text{NRP}}^{95} = 1.6$ keV, with $(R - 1) \sim 0.007$. We know that this bound is accurate because we monitored the evolution of the mass bound versus execution time, and checked

Notice that our 95% CL credible limit on $m_{\rm NRP}$ in ΛWDM models is very close to that obtained from phase-space density arguments [24] applied to newly discovered dwarf spheroidal satellites of the Milky Way [25], which give $m_{\rm NRP} > 1.77\,{\rm keV}$ (see also [34]).

We then ran CosmoMC for the full ΛCWDM model, with one more parameter $F_{\rm WDM}$. Our results are summarized in figure 6. The plots on the diagonal show the probability of each parameter. The plots off-diagonal show the (Bayesian) credible limits (68% CL or 95% CL) on pairs of parameters.

Figure 7 focuses on the two-dimensional probability distribution in the plane $(F_{\rm WDM}, \langle v \rangle_{\rm WDM})$ or $(F_{\rm WDM}, (1{\rm keV})/m_{\rm NRP})$. As $F_{\rm WDM}$ approaches one (pure WDM limit), the 95% CL contour reaches $\langle v \rangle_{\rm WDM} \sim 0.10\,{\rm km/s}$, which corresponds to a lower bound on the mass $m_{\rm NRP}^{95} = 1.6\,{\rm keV}$ (coincidentally, this is identical to the bound derived from the one-dimensional probability of $\langle v \rangle_{\rm WDM}$ in the ΛWDM case). In the opposite limit, as $\langle v \rangle_{\rm WDM}$ grows, we qualitatively expect that the contour will tend towards a constant value, since below a particular value of $F_{\rm WDM}$ the impact of the WDM component on the linear power spectrum will become too small for being detectable by the VHS data, given the error bars and calibration uncertainty of this data. We find indeed that the 95%CL contour reaches asymptotically $F_{\rm WDM} \simeq 0.1$: that is, an admixture of about 10% of WDM with an arbitrary value of the mass within our prior bound ($m_{\rm NRP} \geq 160\,{\rm eV}$) is compatible with the VHS Ly-α data.[8]

6 SDSS results

We now consider the bounds that can be obtained by combining two data sets: WMAP5 [114] and the SDSS Ly-α data introduced in section 3.2. We did not include any other experimental results in this section.

6.1 Pure WDM model

Before applying the method described in section 3.2 to the ΛCWDM model, we updated the analysis of [65] for a pure ΛWDM model. The new ingredients in this work are

(i) the use of WMAP5 rather than WMAP3 data;

(ii) the suggestion of ref. [55] to marginalize the astrophysical parameter γ over a more conservative range (recall γ describes the relation between the local temperature of the intergalactic medium and its local overdensity, $T = T_0(1+\delta)^{\gamma-1}$).

Apart from these new inputs, we performed several tests concerning the validity and robustness of the method, trying different schemes of interpolation between the points where the hydrodynamical simulations were performed, implementing or not thermal velocities in the initial conditions, testing extensively the convergence of MCMCs, and comparing Bayesian and frequentist limits. For these tests we performed GADGET-II simulations for three different values of the mass, $m_{\rm NRP} = 0.5, 5, 10\,{\rm keV}$ (instead of a single one, used in [65]).

that its variations remain negligible (less than 5%) during the second half of the run; also, we checked that if we vary the fraction of points to remove at the beginning of each chain in the range 20-80%, or if we remove one of the chains, the bound remains precisely equal to 1.6 keV. In the next section on SDSS results, we will use CosmoMC with a more convenient convergence criterion than R in order to establish the precision and stability of all 95% CL credible limits

[8]Notice, however, that a ΛCWDM model with 10% of WDM and $m_{\rm NRP} \simeq 160{\rm eV}$ is ruled out by phase-space density considerations [25]. Indeed the bound $m_{\rm NRP} > 1.77{\rm keV}$ presented in [25] scales as $f_{\rm WDM}^{1/3}$. Therefore when reducing the fraction of WDM from 100% to 10%, it diminishes by 50% only and becomes $m_{\rm NRP} > 0.89\,{\rm keV}$.
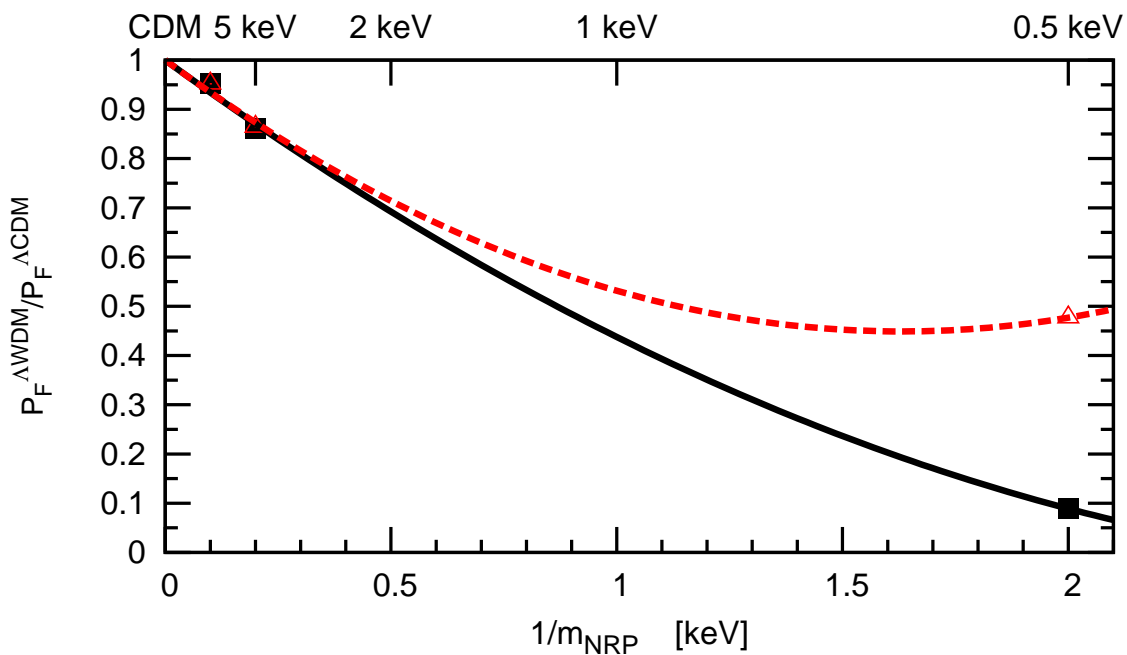
Figure 8. Dependence of the interpolated flux PS of ΛWDM models (divided by that of ΛCDM) on thermal velocities in ICs, here for $k = 0.018 s/km$ and $z = 4.2$. The points are obtained with hydrodynamical simulations; the curves correspond to a global quadratic fit of these points.
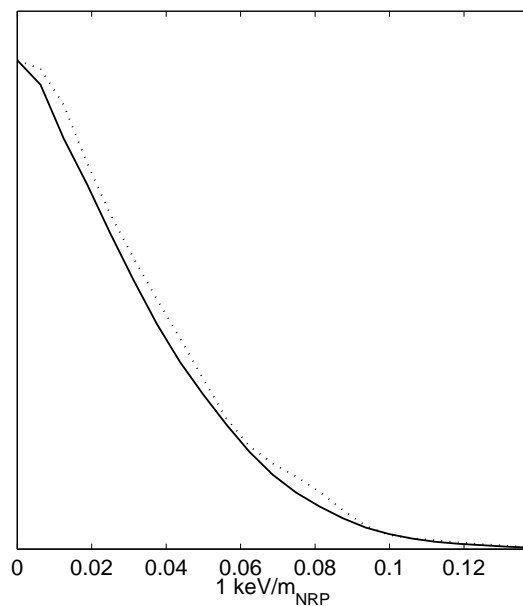
Figure 9. Probability distribution for the parameter $1\,\mathrm{keV}/m_{\mathrm{NRP}}$ (which is identical to $\langle v \rangle_{\mathrm{WDM}}/(157\ \mathrm{m/s})$) in the pure ΛWDM case, using WMAP5 and SDSS Ly-α data, and starting from a flat prior on this parameter; the solid line shows the marginalized posterior, while the dashed line shows for comparison the average likelihood. The normalization of the y-axis (the probability) is arbitrary.

6.1.1 Bayesian credible interval

It is important to check whether including or not thermal velocities into the ICs has an impact on the WDM mass bounds. The analysis of section 4 shows that thermal velocities are expected to change significantly the simulated flux PS at least for $m_{\rm NRP} \lesssim 0.5$ keV, while the effect of velocities remains very small at least for $m_{\rm NRP} \gtrsim 5$ keV. Since previous works [64, 65] obtained a (Bayesian) lower bound of the order of $m_{\rm NRP}^{95} = 10$ keV (95% CL), one expects the influence of thermal velocities in ICs onto the lower mass bound to be small. To analyze this issue in details we performed a number of tests.

In our analysis, the dependence of $P_F^{\Lambda{\rm WDM}}(k, z)$ on $m_{\rm NRP}$ for each value of (k, z) is obtained by interpolation, following a global quadratic fit to the four points for which we have exact results ($m_{\rm NRP} = 10, 5, 0.5$ keV, and the pure ΛCDM case $m_{\rm NRP} = \infty$). The result of such a fit is shown in figure 8 for particular values of k and z. For $m_{\rm NRP} < 5$ keV, the flux PS is strongly affected by the presence or absence of thermal velocities in the hydrodynamical simulations with $m_{\rm NRP} = 0.5$ keV, even with some level of arbitrariness since various interpolation schemes could be used between $m_{\rm NRP} = 0.5$ keV and $m_{\rm NRP} = 5$ keV. Even the values of P_F for $m_{\rm NRP} \geq 5$ keV are slightly affected at the per cent level by the difference between the two interpolations.[9] Thus, the dependence on velocities in ICs can potentially affect the pure WDM result, which depends on the flux spectrum variation for $m_{\rm NRP} \gtrsim 10$ keV.

We have performed MCMC runs for both types of simulated flux PS (with and without thermal velocities in ICs), using a Bayesian top-hat priors on the parameter $0 \leq \langle v \rangle_{\rm WDM} \leq 0.3$ km/s (corresponding to $m_{\rm NRP} \geq 0.5$keV). At the 95% CL, we found $0 \leq \langle v \rangle_{\rm WDM} \leq 11.6$ m/s (with velocities) or $0 \leq \langle v \rangle_{\rm WDM} \leq 11.1$ m/s (without velocities), corresponding to the bounds $m_{\rm NRP}^{95} = 13.5$ keV (with velocities) or $m_{\rm NRP}^{95} = 14.1$ keV (without velocities). In figure 9, we show the marginalized probability distribution for the variable 1 keV$/m_{\rm NRP}$, which is identical to $\langle v \rangle_{\rm WDM}/(157$ m/s$)$ (see equation (4.2) at $z = 0$).

As any credible interval limits obtained with an MCMC method, the above values of $m_{\rm NRP}^{95}$ have some uncertainty related to the fact that there is no clear and unique criterion of convergence for MCMCs [100]. It is always difficult to decide when the bounds are considered to be stable and when to stop CosmoMC. To quantify this ambiguity, we used some convergence criteria implemented into CosmoMC: `MPI_Limit_Converge_Err = 0.3` and `MPI_Limit_Converge = 0.025`, which mean that the run stopped when the 95% CL credible limits were estimated to be accurate at the level of 30% of the standard deviation for each parameter. In the case of $\langle v \rangle_{\rm WDM}$, the standard deviation was found to be $\sigma = 3.6$ m/s, so the error on the bounds coming form the finite degree of convergence of the chains was of the order of ~ 1 m/s. This means that our bounds for the velocity and for the mass are only accurate up to $\pm$ 10%. Indeed, this reflects the typical variations that one observes when varying the fraction of the chains included in the analysis, when removing some of the chains, etc. Including this source of error, the two bounds obtained with and without thermal velocities are found to be compatible with each other, and are summarized by $m_{\rm NRP}^{95} = 12.1$ keV. This final result for the ΛWDM case, which takes into account the systematic uncertainty of the MCMC method, depends neither on the interpolation scheme, nor on the inclusion thermal velocities in ICs.

---

[9] We have also compared different ways of interpolating the flux PS between the four points at our disposal for each (k, z) and found that above $m_{\rm WDM} \gtrsim 5$ keV, the difference between the various interpolation schemes is at most of the order of several per cents for each $P_F^{\Lambda{\rm CWDM}}(k, z)$, which is comparable with the error bars on the data points of the SDSS set. The resulting errors in $m_{\rm NRP}^{95}$ are less than 10%.

Run	$-\log(\mathcal{L}_{\mathrm{best}})$	$2\Delta\log(\mathcal{L}_{\mathrm{best}})$	# params.	Comment
CDM $(\Leftrightarrow m_{\mathrm{NRP}} = \infty)$	1404.0	0.0	33	
WDM, $m_{\mathrm{NRP}} = 13.5\,\mathrm{keV}$	1404.6	1.2	33	$m_{\mathrm{NRP}} = m_{\mathrm{NRP}}^{95}$
WDM, $m_{\mathrm{NRP}} = 11.2\,\mathrm{keV}$	1405.2	2.4	33	$m_{\mathrm{NRP}} = m_{\mathrm{NRP}}^{95}/1.2$
WDM, $m_{\mathrm{NRP}} = 9.0\,\mathrm{keV}$	1406.3	4.6	33	$m_{\mathrm{NRP}} = m_{\mathrm{NRP}}^{95}/1.5$
WDM, $m_{\mathrm{NRP}} = 6.75\,\mathrm{keV}$	1412.0	16.0	33	$m_{\mathrm{NRP}} = m_{\mathrm{NRP}}^{95}/2.0$

Table 1. Dependence of the best likelihood in our MCMCs (for SDSS Lyman-α and WMAP5 data) on the mass m_{NRP}. The five lines correspond to distinct sets of chains, obtained by running CosmoMC with *fixed* values of m_{NRP}: CDM limit (equivalent to $m_{\mathrm{NRP}} = \infty$), and m_{NRP} equal to m_{NRP}^{95} divided by 1, 1.2, 1.5 and 2.0, where m_{NRP}^{95} is the mass value corresponding to the Bayesian 95% CL upper bound on $\langle v \rangle_{\mathrm{WDM}}$. Notice that these five cases have the same number of degrees of freedom (data points minus parameters).
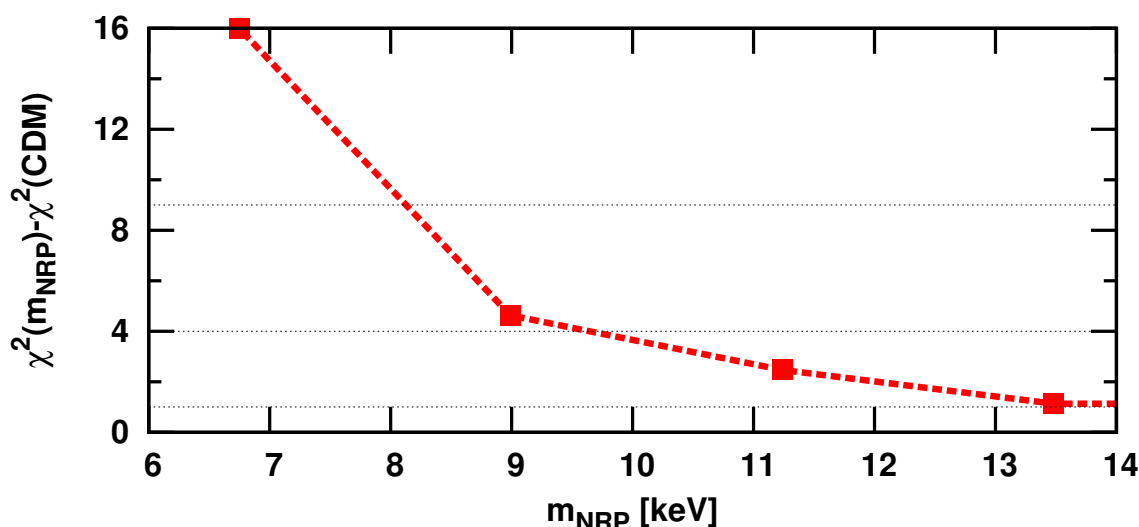
Figure 10. Dependence of $\Delta\chi^2 = -2\log\mathcal{L}$ on the WDM mass m_{NRP}. The values are taken from table 2, and the dashed line linearly interpolates between the points.

This discussion suggests that in the mixed ΛCWDM case, we should use a top-hat prior $0 \le \langle v \rangle_{\mathrm{WDM}} \le 0.03$ km/s (corresponding to $m_{\mathrm{WDM}} \ge 5$ keV) in order to obtain conservative bounds; in this way, our final results will not depend on the treatment of thermal velocities; and more importantly, they will not be affected by the interpolation scheme, which would remain somewhat arbitrary even if the thermal velocities were correctly implemented in GADGET. In order to obtain robust results below $m_{\mathrm{WDM}} \sim 5$ keV, one should perform more hydrodynamical simulations for intermediate values of the mass, and perform extensive tests of the convergence of GADGET results w.r.t thermal velocity effects. This analysis is beyond the scope of the present work.

6.1.2 Comparison with frequentist approach

In the previous section, we found that the 95% CL credible interval for $\langle v \rangle_{\mathrm{WDM}}$ corresponds to a lower limit on the mass $m_{\mathrm{NRP}}^{95} = 13.5$ keV (not including the additional uncertainty related to MCMC convergence issues, which led us to lower the final bound to $m_{\mathrm{NRP}}^{95} = 12.1$ keV).

It is well known that the Bayesian approach finds the *most probable* parameter values given the data (see appendix A for a short introduction to Bayesian and frequentist analyses). Therefore the Bayesian 95% CL limits on each parameter border the region containing 95% of the parameter probability (marginalized over other parameters). We are also interested in the answer to a different question: whether for a particular value of $m_{\rm NRP}$ there exists *at least one model* which fits the data well enough compared to pure CDM (regardless of *how many models* fit the data equally well). Addressing this question is particularly useful for *excluding* conservatively some values of the mass, since it also tells beyond which value *there is not a single model* providing a good fit to the data.

If the likelihood of the ΛWDM model was a perfect multivariate Gaussian, we would expect that $m_{\rm NRP}^{95}$ is the value of the mass for which the maximum likelihood ($\max[\mathcal{L}|_{m=m_{\rm NRP}^{95}}]$) is equal to the absolute maximum ($\max[\mathcal{L}]$) times e^{-2}. In the general case, this is not necessarily the case, and the frequentist bounds can differ significantly from the Bayesian ones.

To estimate the frequentist confidence limits on $m_{\rm NRP}$, we performed a number of CosMoMC runs with fixed values of the mass. In table 1, we quote the maximum likelihood in each set of chains. Variations in the logarithm $-2\log(\mathcal{L}_{\rm best})$ (which would be χ^2-distributed in the limit of a multivariate Gaussian) can be interpreted as variations in the goodness-of-fit for each value of the mass. By looking at table 1, one sees that the best-fit model for $m_{\rm NRP} = 13.5$ keV fits the data almost as well as the pure CDM model (the differences $\Delta\chi^2 = 1.2$ is not statistically significant).

As mentioned in appendix A, the value of the mass for which $-2\log(\mathcal{L}_{\rm best})$ worsens by $\Delta\chi^2 = 4$ (resp. $\Delta\chi^2 = 9$) is an approximation for the 95%CL (resp. 99.7%CL) lower bound for $m_{\rm NRP}$, conventionally quoted as the 2σ (resp. 3σ bound) in many data analyses based on the frequentist approach. In our case, this happens for $m_{\rm NRP} \simeq 9.5$ keV (2σ bound) and $m_{\rm NRP} \simeq 8$ keV (3σ bound) using linear interpolation. Hence, $m_{\rm NRP} \simeq 8$ keV appears to be a robust 3σ lower bound on the WDM mass (NRP case) in the pure ΛWDM case.

The above derivation of frequentist bounds could be improved by studying more values of the mass, finding the maximum likelihood with higher accuracy, and computing the exact values of $\Delta\chi^2$ corresponding to 95% and 99.7% bounds (for non-Gaussian distributions, these are not exactly equal to 4 and 9). However, we believe that our treatment is sufficient for concluding that values $m_{\rm NRP} \gtrsim 8$ keV are allowed by present data at the 3σ level.

6.2 SDSS results for CWDM

In order to analyze the full ΛCWDM model, we performed extra GADGET-II simulations for a grid of points with $m_{\rm NRP} = 5, 10$ keV and $F_{\rm WDM} = 0.2, 0.5, 0.9$. We have seen that for such values of the mass, thermal velocities in the ICs can be neglected. Hence, we treated the cold plus hot mixture as a single species with no thermal velocities, distributed initially according to the appropriate linear power spectrum computed by CAMB at $z = 99$. Including ΛCDM and ΛWDM models on the edges, we have a total grid of 3×5 models with $m_{\rm NRP} = 5$ keV, 10 keV, ∞ and $F_{\rm WDM} = 0, 0.2, 0.5, 0.9, 1$. For each pair (k, z), we find the value of $P_F^{\Lambda{\rm CWDM}}$ at any given point $(m_{\rm NRP}, F_{\rm WDM})$ by bilinearly interpolating within this grid.

6.2.1 Bayesian credible region

Having performed extensive tests for the case of pure ΛWDM models, we applied the same type of analysis to the full ΛCWDM model. We ran CosMoMC varying all parameters, including $0 \le \langle v \rangle_{\rm WDM} \le 0.03$ km/s (corresponding to $m_{\rm NRP} \ge 5$ keV) and $0 \le F_{\rm WDM} \le 1$. The resulting two-dimensional joint probabilities are shown in figure 11 and figure 12. The
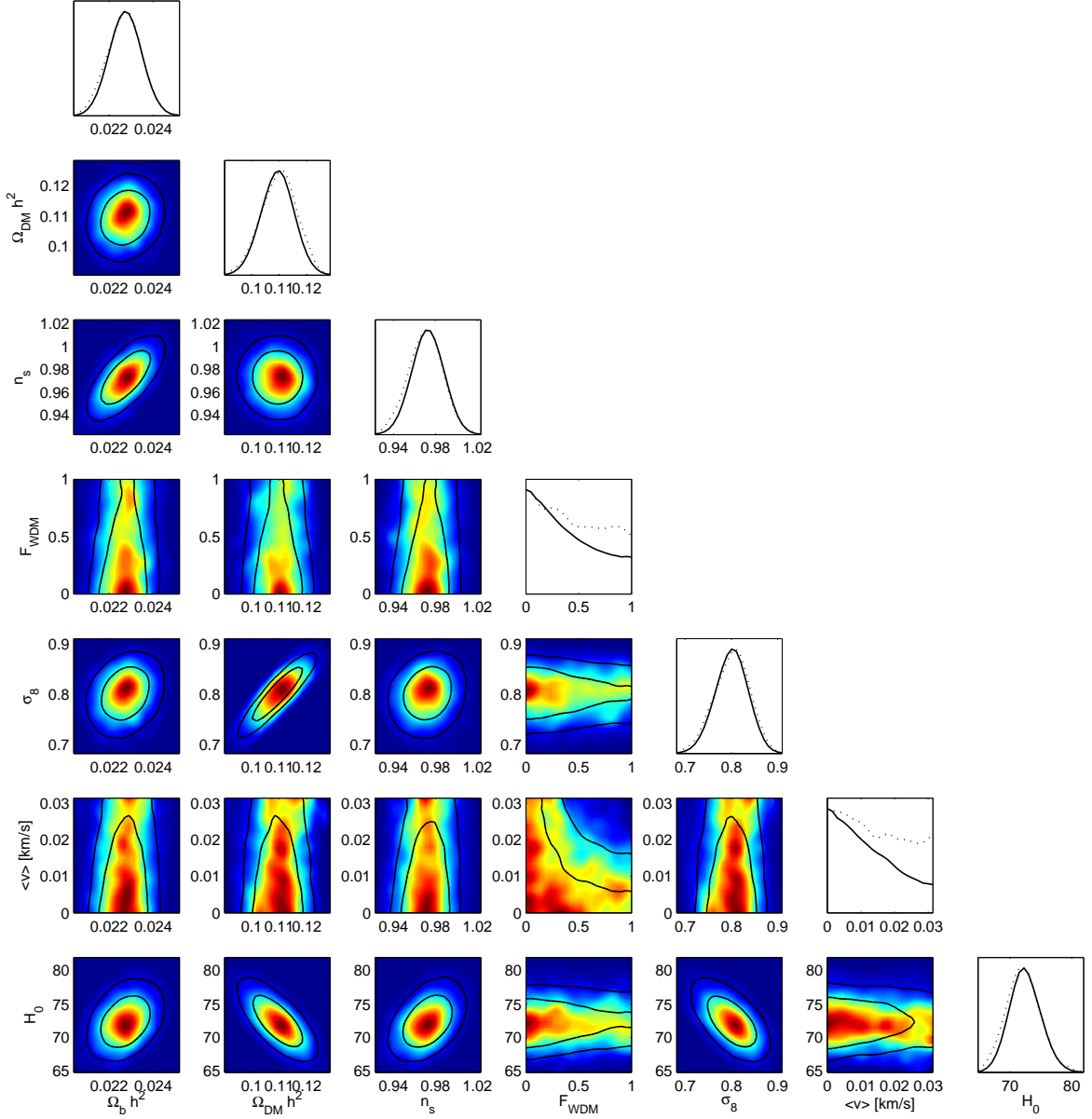
Figure 11. Preferred region for pairs of cosmological parameters in the ΛCWDM model, using SDSS Ly-α and WMAP5 data sets. The black lines represent the 68%CL and 95%CL contours of the two-dimensional probability marginalized over other parameters (as defined in the Bayesian approach), while the colors show the likelihood averaged over other parameters. The five parameters $\Omega_B h^2$, $\Omega_{DM} h^2$, n_s, F_{WDM}, $\langle v \rangle_{WDM}$ have flat priors over the displayed range. Our analysis also assumes flat priors on the logarithm of the primordial spectrum amplitude and on the angular diameter of the sound horizon, but instead of these parameters we show here σ_8 and H_0, which have a more straightforward interpretation. In this plot, we do not show the reionization optical depth τ and all the astrophysical or nuisance parameters entering into the analysis. The one-dimensional marginalized probabilities are displayed along the diagonal.

data clearly prefers the pure ΛCDM limit, which corresponds to the two axes $F_{WDM} = 0$ and $\langle v \rangle_{WDM} = 0$, but significant deviations from this model are still perfectly allowed by the data.
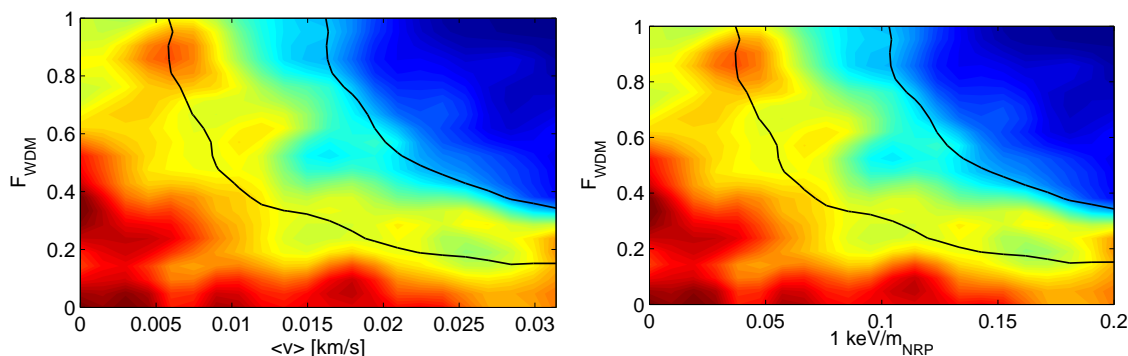
Figure 12. *(Left)* Preferred region for the parameters $(F_{\text{WDM}}, \langle v \rangle_{\text{WDM}})$ of the ΛCWDM model, using SDSS Ly-α and WMAP5 data sets. The black lines represent the 68%CL and 95%CL contours of the two-dimensional probability marginalized over other parameters (as defined in the Bayesian approach), while the colors show the likelihood averaged over other parameters. *(Right)* Same plot with the horizontal axis translated in terms of $(1\text{keV}/m_{\text{NRP}}) = \langle v \rangle_{\text{WDM}}/(157 \text{ m/s})$, see equation (4.2).

One can see that as F_{WDM} approaches one, the 95%CL limit on $(F_{\text{WDM}}, (1 \text{ keV}/m_{\text{NRP}}))$ tends towards $(1\text{keV}/m_{\text{NRP}}) = 0.1$, i.e. $m_{\text{NRP}} = 10$ keV. This bound is weaker than the 12.1 keV limit obtained in the pure ΛWDM analysis, because it is derived from a joint two-dimensional probability.[10] There is a number of models with $F_{\text{WDM}} < 1$ and masses of the order of 5 keV to 10 keV which lie in the region preferred by the data. In particular, for F_{WDM} lower than 35%, the data is compatible with the smallest mass included in our prior range ($m_{\text{NRP}} = 5$ keV). We did not include smaller masses in the analysis for the reasons explained at the end of section 6.1.1, but it is interesting to see that for $m_{\text{NRP}} \sim (5-7)$ keV the bound on F_{WDM} reaches a flat asymptote; this suggests that for such a small WDM fraction, the amplitude of the suppression in the small-scale flux power spectrum is so small that the Ly-α data is compatible with any arbitrary value of the free-streaming scale. In this case, considerably smaller masses are likely to be allowed, and we would in fact need to add data on larger scale (like galaxy redshift surveys) in order to better constrain the free-streaming scale and the mass. This would lead to mass limits corresponding to hot dark matter rather than warm dark matter particles.

6.2.2 Comparison with frequentist approach

Similarly to section 6.1.2 we have performed a number of CosmoMC runs on a grid of points with $m_{\text{NRP}} = 5, 10$ keV and $F_{\text{WDM}} = 0.2, 0.5, 0.9, 1.0$, varying the same parameters as in the pure ΛCDM case. For each of these runs, we report in table 2 the value of $-\log(\mathcal{L}_{\text{best}})$ in our chains, which plays the role of $\chi^2/2$. The dependence of χ^2 on F_{WDM} for $m_{\text{NRP}} = 5$ keV is presented in figure 13. We see that if the mass is assumed to take this particular value, the 2σ confidence limit ($\Delta\chi^2 = 4$) becomes $F_{\text{WDM}} \simeq 40\%$, while the 2σ limit ($\Delta\chi^2 = 9$) allows for about 60% of WDM. We can try to compare this case with the results of our Bayesian analysis, for which the joint 95% CL limit on $(F_{\text{WDM}}, (1 \text{ keV}/m_{\text{NRP}}))$ reaches $F_{\text{WDM}} = 0.35$ in the limit $m_{\text{NRP}} = 5$ keV. In the frequentist approach, the joint 95% CL on a pair of parameters is approximated by $\Delta\chi^2 = 6.2$. This corresponds to an upper bound $F_{\text{WDM}} \simeq 0.50$, less

---

[10]The 95%CL limit in figure 12 contains 95% of the posterior probability in the full $(F_{\text{WDM}}, (1 \text{ keV}/m_{\text{NRP}}))$ plane. It is clearly different to look for the restriction of this limit to $F_{\text{WDM}} = 1$, and to compute the range containing 95% of the posterior probability along the $F_{\text{WDM}} = 1$ axis.

m_{NRP} F_{WDM}	CDM	10 keV	5 keV
1.0 (WDM)	1404.0	1405.8	1415.8
0.9	1404.0	1406.4	1413.2
0.5	1404.0	1404.1	1407.4
0.2	1404.0	1404.1	1404.1
0.0 (CDM)	1404.0	1404.0	1404.0

Table 2. Values of $-\log(\mathcal{L}_{\mathrm{best}})$ (which play the role of $\chi^2/2$) for runs with fixed m_{NRP} and F_{WDM}. All runs have the same number of parameters, equal to that of CDM.
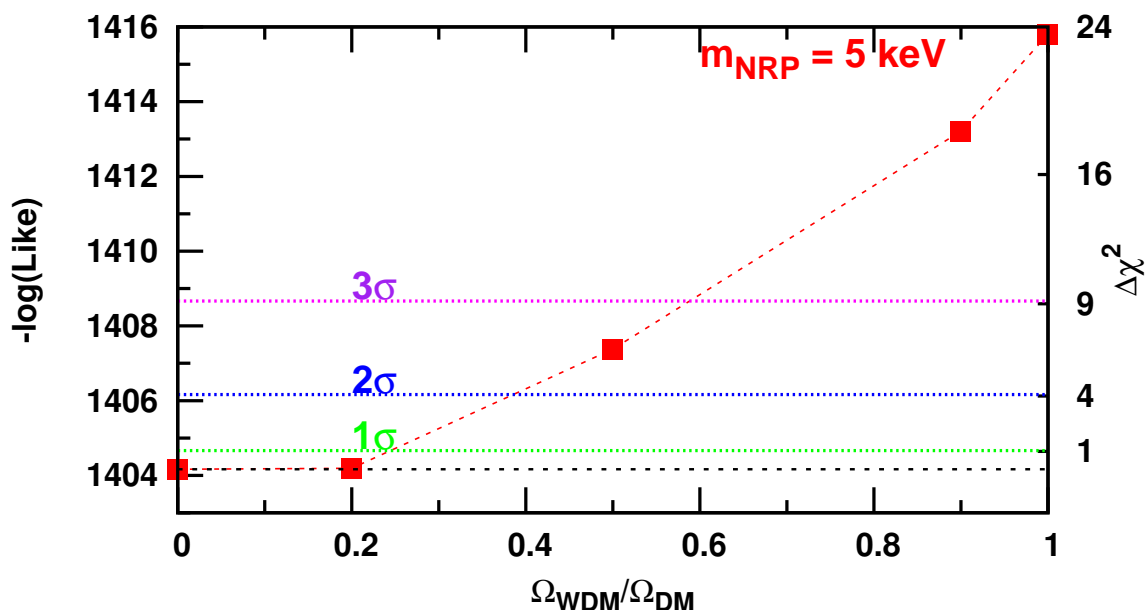
Figure 13. Dependence of $-\log(\mathcal{L}_{\mathrm{best}})$ on F_{WDM}, assuming that the mass is fixed to $m_{\mathrm{NRP}} = 5\,\mathrm{keV}$. Horizontal dashed lines show the levels $\Delta\chi^2 = 1, 4, 9$, corresponding to the $1, 2, 3\sigma$ confidence limits.

restrictive than the comparable Bayesian limit. For $m_{\mathrm{NRP}} = 10\,\mathrm{keV}$, all values of the WDM fraction (up to pure ΛWDM) are allowed, in agreement with the results of section 6.1.2.

7 Systematic uncertainties

The bounds derived previously assume that all systematic uncertainties are properly taken into account in the WMAP5, VHS and SDSS Ly-α data likelihoods implemented in Cos-moMC. Systematic errors are of course hard to estimate. Here, we want to summarize the assumptions concerning systematic errors on which our results are based, and to describe a number of related tests.

The systematic uncertainties entering into our final mass bounds can be roughly subdivided into:

1. *Observational* uncertainties related to the way the Ly-α forest data are processed to extract the flux power spectrum. Among these uncertainties the most important

are: *i*) mean flux level of the data sets, which could be different from data set to data set and is usually kept as a free parameter to marginalize over in a reasonable range of observed values (e.g. [123]); *ii*) the continuum of the distant QSOs, which is either subtracted from the data (e.g. [61]) or implicitly removed by considering only a smaller portion of the spectra where the continuum is not contributing to the flux power (e.g. [104]); *iii*) the metal absorption systems in the Ly-α forest, whose contribution to the flux power could be estimated from Voigt profile fitting statistics for high-resolution spectra [104] or modelled using the framework proposed by [61] for low-resolution spectra; *iv*) the contribution to the flux power due to the damping wings of strong damped Ly-α systems (DLAs) which again can be either removed (VHS) or modelled with the help of hydro simulations (SDSS); *v*) uncertainties in the noise level and resolution of the instrument, which is particularly important for the SDSS data set. We stress that among all these uncertainties the first two are the most important, while the metal line contribution and the presence of DLAs is modelled using parameters (constrained with priors) that are varied in the MCMC method. We refer to the extensive analysis made in refs. [61, 108] for a more quantitative discussion on the systematic errors and in the raw data processing technique.

2. *Theoretical* uncertainties, related to *numerical* simulations, such as the finite box size and finite numerical resolution. These are usually addressed by running a number of simulations that explore further the parameter space in resolution and box-size and checking the impact on the flux power. Note that these corrections are of course code-dependent and could be different in Eulerian and Lagrangian code. For a comparison between different codes we refer to [103]. It is also important to compare the full hydrodynamical simulations with other less time consuming hydro schemes such as the HPM that have been used by several authors. The agreement between the Eulerian code ENZO and the Lagrangian code GADGET-II in terms of flux power is found to be below or around the 5% level [103], while the discrepancy between GADGET-II and HPM [124] could be as high as 20-30% (in the low redshift bins, while at higher redshift is usually better and at the percent level) as found in [102]. A quantitative analysis of Ly-α flux and line properties using the code ENZO has also been made in [125] with a particular focus on box-size and resolution problems.

3. *Astrophysical* uncertainties relevant for Ly-α physics, e.g. concerning the thermal history and ionization history of the IGM. One of the key parameters describing the influence of the IGM on the flux power spectrum is γ, which appears in the empirical relation $T = T_0(1+\delta)^{\gamma-1}$ between density fluctuations and the IGM temperature. Recent results of [55] suggested an inverted temperature-density relation (i.e. the possibility of having $\gamma < 1$). In order to derive conservative bounds, it was suggested in [55] to marginalize γ over a wide range, including values below $\gamma = 1$. In this case, the effect of γ on the flux power spectrum is not necessarily captured by a linear approximation, and one should use at least a second order Taylor expansion of $P_F(k,z)$ as a function of γ [55, 66]. The results of this paper assume a wide range and a second-order Taylor expansion for γ, as in these last references. This issue is particularly relevant for ΛWDM and ΛCWDM analyses, because the the effect of changing the density-temperature relation can be somewhat degenerate with that of introducing a cut-off in the primordial matter power spectrum. Indeed, we found that implementing the old method used in [63, 65] ($\gamma > 1$, first order Taylor expansion of P_F in γ) affects our results for the mass bound

m_{NRP}^{95} by about 20%. Since the density-temperature relation issue is not fully settled yet, we consider the uncertainty on γ to be one important source of systematic errors in our analysis. Another physical ingredient which is particularly important and so far has been poorly modelled in hydrodynamical simulations is the reionization of hydrogen (which is related to the filtering scale of the IGM, see for example [49]): estimates give a few percent impact on the SDSS flux power but radiative transfer effects (that are likely to generate temperature and ionization fluctuations at large scales) need to be better understood in order to quantify the effect on the flux power at several scales and redshifts at a level comparable to the statistical error of the data [92, 126]. In principle all the physical processes that could impact on the flux power at large scales (roughly above few Mpc) need to be considered: galactic winds, star formation, cosmic rays, Active Galactic Nuclei (AGN) feedback, etc. (see e.g. [60, 105, 108, 127]). However, we must stress that: i) accurate investigations made with hydrodynamical simulations show that the impact of these effects at large scales is either minimal or degenerate with other parameters of the thermal history that are marginalized over; ii) the effect of a warm dark matter component on the flux power spectrum does not seem to be very degenerate with other physical/cosmological parameters (at least in the ΛWDM case), see e.g. [64].

4. Uncertainties related to the parameter extraction method. As discussed already in sections 5 and 6.1.1, the ambiguity of defining a stopping criteria for the MCMCs (corresponding to a given degree of convergence of the chains) can lead to significant errors in the bounds. This error can always be reduced by increasing the length of the chains, but for models like ΛCWDM for which the execution time of CAMB is larger than usual (due to the necessity of including several discrete momenta in the evolution equations of the warm component), reaching a very high degree of convergence quickly becomes prohibitive in terms of CPU time. The error on the bounds can be estimated by CosmoMC itself, as already mention in the result sections. It should always be included when quoting results from CosmoMC. For instance, it lead us to write our ΛWDM mass bound for the SDSS case as m_{NRP}^{95}=12.1 keV instead of 13.5 keV.

5. Finally, there are also uncertainties related to the CMB data. For instance, it is well-known that a different treatment of systematic errors in WMAP5 (beam shape, small-l likelihood, etc.) has led to a shift of the allowed range of some parameters with respect to WMAP3 (e.g. σ_8). However, the results of figure 11 show that the parameters describing the warm sector are not degenerate with other cosmological parameters, and should therefore be rather insensitive to changes in the CMB data.

In summary, our estimates are based on the current state-of-the art concerning the modelling of systematic errors involved in this field. We checked many of these assumptions with designated test runs and found that the bounds remain intact within $\approx 30\%$ uncertainty. Of course, the number of assumptions is such that derived bounds should be considered with care. As an illustration of this, the mass bound obtained by Seljak et al. [64] and Viel et al. [65] for the same model (pure ΛWDM) and data set (SDSS Ly-α plus CMB data) differ by 30% due to variations in the treatment of systematics, data interpretation, numerical issues, etc.

8 Conclusion

In this work we have performed a thorough analysis of Ly-α constraints on warm and cold plus warm DM models using WMAP5 data, combined with VHS or SDSS Ly-α data. As
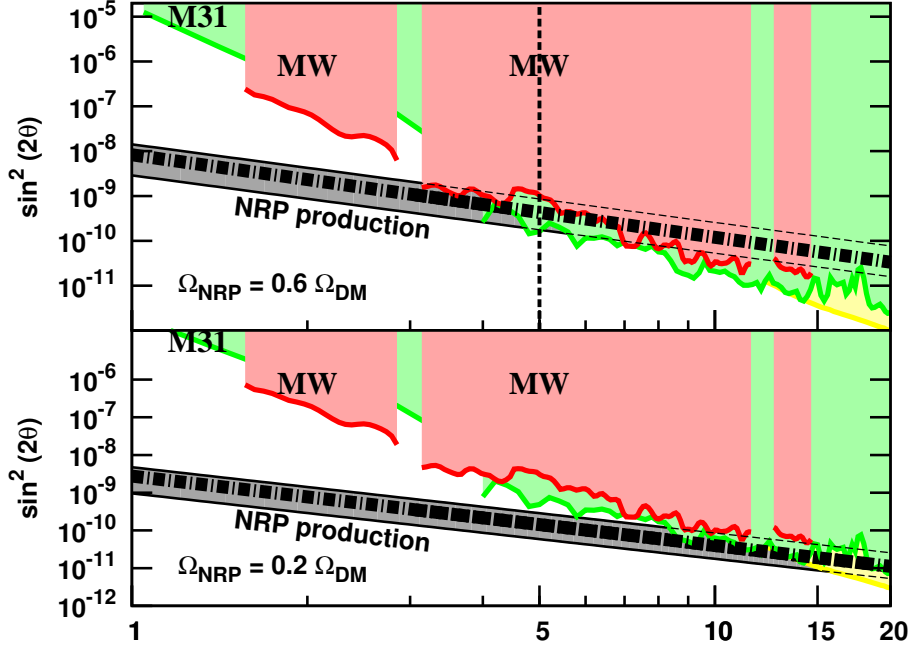
Figure 14. Comparison of X-ray bounds with the results of our Ly-α analysis of ΛCWDM, for the case in which NRP sterile neutrinos contribute to 60% (upper panel) or 20% (lower panel) of the dark matter density. The wide gray band (labeled "NRP production") shows the results of the computation of the NRP sterile neutrino abundance, taking into account uncertainties from QCD (see [80, 128] for details). The X-ray bounds are from [45] (label "MW"), from [129] (label "M31") and from [41] (yellow region in the lower right corner). To account for possible uncertainties in the determination of the DM amount in various object, the X-ray bounds have been rescaled by a factor of 2 (c.f. [129]). The vertical dashed line marks the 5 keV lower bound on the mass found in the present analysis, assuming 60% of WDM. For 20% of DM, we found that the mass remains unconstrained by Ly-α data.

expected from the quality of the data, the results based on SDSS Ly-α data are much more constraining, and below we only summarize this case.

Our results apply to any model in which the phase space distribution of the warm component can be approximated by a Fermi-Dirac or rescaled Fermi-Dirac distribution. The latter case (assuming a temperature $T = T_\nu$) is a first-order approximation for the case of non-resonantly produced sterile neutrinos. In most of the paper, we expressed our mass bounds in terms of the mass m_{NRP} defined in this case.

Within a conservative frequentist approach, for pure ΛWDM models, masses m_{NRP} below 8 keV are excluded at 99.7% CL ($m_{\mathrm{NRP}} \geq 9.5$ keV at 95% CL). In the case of CWDM models, our analysis shows that for $m_{\mathrm{NRP}} = 5$ keV (the smallest WDM mass probed in this investigation) as much as 60% of WDM is allowed at 99.7% CL (40% at 95% CL). We believe that these results are robust within the current state-of-the-art. Of course, as the Ly-α method is still being developed, these results could be affected by still unknown systematic uncertainties (see discussion in the section 7).

From the same data we have also obtained Bayesian credible intervals on the same parameters. The bound on m_{NRP} (at 95% CL), defined as in previous works [63–65]), are $m_{\mathrm{NRP}} \geq 12.1$ keV for pure ΛWDM; for ΛCWDM, the joint probability of $(F_{\mathrm{WDM}}, 1/m_{\mathrm{NRP}})$ is displayed in figure 12: this shows that for the smallest probed mass 5 keV, the data is

compatible with $F_{\mathrm{WDM}} \leq 35\%$.

Our results can be easily translated for the case thermal relics, the corresponding limits are the following. In the frequentist framework, for pure ΛWDM, masses m_{TR} below $1.5\,\mathrm{keV}$ are excluded at 99.7% CL ($m_{\mathrm{TR}} \geq 1.7\,\mathrm{keV}$ at 95% CL). In the case of CWDM models, our analysis shows that for $m_{\mathrm{TR}} = 1.1\,\mathrm{keV}$ (the smallest WDM mass probed in this investigation) as much as 60% of WDM is allowed at 99.7% CL (40% at 95% CL). In the Bayesian approach, for pure ΛWDM, the 95% CL bound defined in the same way as before reads $m_{\mathrm{TR}} \geq 2.1\,\mathrm{keV}$. For the ΛCWDM, the joint constraints on the mass and on the warm fraction can be easily obtained from the left plot in figure 12, translated in terms of m_{TR} using equation (4.1).

Let us now discuss the implications of our results for models in which the dark matter (or part of it) consists of non-resonantly produced sterile neutrinos.

The lower mass bound for the pure ΛWDM case should be compared with X-ray bounds [41, 43–47, 129–132], that restrict the mass of NRP sterile neutrinos from above. Confronting the upper bound $m_{\mathrm{NRP}} \leq 4\,\mathrm{keV}$ (see e.g. ref. [129]) with the bound $m_{\mathrm{NRP}} \geq 8\,\mathrm{keV}$ obtained in this work (both at 99.7% CL) excludes the NRP scenario. Again, this conclusion should be taken with care in view of the above discussion of systematic errors.

Next, we analyze the case of mixture of NRP sterile neutrino and some other, cold DM particle (similar to [90]). To this end, one should rescale the X-ray constraints of [41, 43–47, 129–132] and the results of the NRP DM abundance computation [80, 128] by a factor $F_{\mathrm{WDM}} < 1$. We can compare the upper bounds rescaled in this way with the results of our CWDM runs (see figure 14). We see that for $F_{\mathrm{WDM}} \geq 0.6$, SDSS Ly-$\alpha$ bounds are in conflict with X-ray constraints at 99.7% CL. For an NRP fraction $F_{\mathrm{WDM}} = 0.4 - 0.6$, an allowed window for the mass appears around $m_{\mathrm{NRP}} \approx 5\,\mathrm{keV}$ (c.f. figure 14, upper panel). For smaller F_{WDM}, the upper mass bound from X-rays quickly increases (as the lower panel of figure 14 demonstrates). At the same time, given that 1 and 2σ Ly-α contours for F_{WDM} become horizontal as m_{NRP} approaches 5 keV (c.f. figure 12), we expect that masses smaller than 5 keV with $F_{\mathrm{WDM}} \lesssim 0.4$ should be allowed (although a precise analysis should properly take into account thermal velocities, c.f. section 4). Thus, we conclude that for $F_{\mathrm{WDM}} < 0.6$ a window of allowed NRP masses opens up, and for $F_{\mathrm{WDM}} \sim 0.2$ we see that all masses (above the phase-space density bound [25]) are allowed up to ~ 15 keV.

Another DM model which has similarities with the ΛCWDM scenario discussed here is that of resonantly produced sterile neutrinos [78, 81, 83]. In this case, the DM velocity dispersion has a colder (resonant) and a warmer (NRP produced) component. In this case, a specific analysis is needed in order to apply the results of this work. We will present these results elsewhere [133].

Further improvements in the results presented here would require performing simulations for a larger grid of points $(m_{\mathrm{NRP}}, F_{\mathrm{WDM}})$, with a better control of systematics as well as better understanding of the physics of the IGM. Ideally, one would like to fit all the IGM statistics at once (flux power spectrum, flux probability distribution function, flux bispectrum and all the line-based statistics) in the spirit of [55, 134] to find a consistent IGM model from low to high redshifts.

High redshift QSOs are important for WDM (and any matter power spectrum related) investigations, since at higher redshifts the structures are more linear and should more closely resemble the underlying matter power spectrum. However, at $z > 5$ the IGM becomes more neutral and the mean flux level lowers. Thus, interpreting the almost saturated spectra would require hydrodynamical simulations at much higher resolution in order to account for very small structures that contribute to absorption. Furthermore, the number density of QSOs

drops significantly at high redshifts and thereby the progress will be somewhat limited also in a statistical sense.

In principle, QSO spectra (especially those at high resolution and with high signal-to-noise) carry information down to scales comparable to the resolution element (for VLT, Very Large Telescope, UVES-spectra ~ 0.02 Å which could be roughly translated into 200 h^{-1} comoving kpc at $z = 3$), thereby starting to probe the sub-Mpc scales. Although these numbers are very promising, it is important to stress that at these scales the flux power spectrum becomes very steep, so that a small change in the astrophysical and cosmological parameters could have a large impact on it. To interpret it with hydrodynamical simulations could become challenging both for resolution and physical issues (all the physical ingredients that could have an influence on galactic scales need to be modelled and their effect re-computed). It is probably more promising to tackle some physical effects such as the IGM thermal evolution with independent probes (like line statistics) and use them as strong priors in the interpretation of the flux power at small scales, in order to restrict the parameter space. A large number of intermediate resolution QSO spectra, between that of SDSS and VLT spectra, will be also very important in order to cross-check the effects of systematics on the data and improve the limits obtained in this work. This effort could be possible quite soon with the X-shooter spectrograph [135].

A Confidence vs. credible interval

The main goal of this project is to obtain reliable bounds on the parameters of some particle physics DM models, based on the cosmological observations of the Ly-α forest. This requires a careful examination of the notion of *confidence limits* in the context of particle physics and cosmology. An extended discussion of this subject is beyond the scope of this paper, see e.g. [136], or [137]. For a short introduction see [138].

In particle physics one can usually repeat an experiment to determine the value of a parameter p. The measured data is a fluctuating random variable. Then, for example, the 95% *confidence interval* on a parameter p is defined as the answer to the following question: "What is the interval within which the parameter p will lie in 95% of all measurements?" This approach (often called the "frequentist" one) is well suitable for ruling out models.

In cosmology one needs to address a different problem, because we can only make measurements in our observable Universe, i.e. in a single realization of an underlying statistical model. In the Bayesian approach one defines, first, the likelihood $\mathcal{L}(D, \{p_i\})$ of a data set D given a model with parameters $\{p_i\}$, and then the Probability Density Function (PDF) $\Pi(\{p_i\})$ of the parameter set $\{p_i\}$, which is equal to the likelihood $\mathcal{L}(D^{\mathrm{obs}}, \{p_i\})$ (seen as a function of the parameters, with the data fixed to the observed ones) times the prior distribution of each parameter [139–141]. Thus, ultimately, the parameters (not the data!) are treated as a random variables. For each parameter p_i, one can construct a probability $\mathcal{P}_B(p_i)$ by marginalizing (i.e., integrating) $\Pi(\{p_i\})$ over other parameters $p_{j\neq i}$, and defines the *credible interval* as the interval of p_i containing 95% of the probability $\mathcal{P}_B(p_i)$.

However, it is possible to estimate the frequentist *confidence limits*, starting from the same likelihood function. For each parameter p_i, one can maximize the likelihood over the other parameters, which gives an (unnormalised) probability distribution $\mathcal{P}_F(p_i) = \max_{p_{j\neq i}} \mathcal{L}(D^{\mathrm{obs}}, \{p_i\})$. The 95% confidence limits on p_i are defined in such way that inside the corresponding interval, $\mathcal{P}_F(p_i)$ is greater than some number such that 95% of possible data sets lead to a likelihood greater than this number.

In general, the two intervals (frequentist and Bayesian) do not coincide. However, in cosmology, most authors compute Bayesian intervals and call them confidence limit. This is the case of all recent bounds on the WDM mass [63–66]. However, in this paper, we want to carry the Bayesian and frequentist analyses in parallel.

The Monte-Carlo Markov Chain (MCMC) method with Metropolis-Hastings algorithm [100, 139, 141, 142], implemented in the code CosmoMC [100], became a standard method for exploring the Bayesian PDF $\Pi(\{p_i\})$, which is equal to the likelihood $\mathcal{L}(D^{\mathrm{obs}}, \{p_i\})$ (modulo a normalization factor) in case of flat priors. The MCMC method is very effective in scanning Π (or $\mathcal{L}$) in the region where this function is the largest, with the crucial property that once the chains have converged, the density of points in parameter space is proportional to $\Pi(\{p_i\})$. This makes it an ideal tool for a Bayesian statistical analysis (see e.g. [141] and references therein), since the credible interval for a given parameter marginalized over other parameters is simply obtained by counting the number of chain points in each parameter bin.

In order to obtain frequentist confidence limits on a parameter p_i, we should take into account the exact form of the likelihood as a function of the data (in cosmology, the likelihood is usually non-Gaussian, in particular for small-scale CMB data). Instead, we choose to use the same approximation as in many frequentist analyses: we define a χ^2 function as $\chi^2(p_i) = \min_{p_{j\neq i}}[-2\ln\mathcal{L}]$, search for its minimum $\chi^2_{\min} = \min_{p_i}[\chi^2(p_i)]$, and finally define the $1\sigma, 2\sigma, 3\sigma$ confidence intervals as the region in which $\Delta\chi^2(p_i) \equiv \chi^2(p_i) - \chi^2_{\min}$ is smaller than $1, 4$ and 9. In order to minimize $[-2\ln\mathcal{L}]$ over $p_{j\neq i}$, we still use CosmoMC with p_i kept fixed to different values. It is well-known that the CosmoMC algorithm is not optimal for minimization (with respect, e.g., to a simulated annealing method), but in this work it turned out to be efficient enough.

References

[1] S.C. Novati, *Microlensing in galactic halos*, *Nuovo Cim.* **122B** (2007) 557 [`arXiv:0711.4474`] [SPIRES].

[2] Y.B. Zel'dovich, *Gravitational instability: an approximate theory for large density perturbations*, *Astron. Astrophys.* **5** (1970) 84 [SPIRES].

[3] G.S. Bisnovatyi-Kogan, *Cosmology with a nonzero neutrino rest mass*, *Astron. Zh.* **57** (1980) 899.

[4] J.R. Bond, G. Efstathiou and J. Silk, *Massive neutrinos and the large-scale structure of the universe*, *Phys. Rev. Lett.* **45** (1980) 1980 [SPIRES].

[5] A.G. Doroshkevich, M.I. Khlopov, R.A. Sunyaev, A.S. Szalay and I.B. Zeldovich, *Cosmological impact of the neutrino rest mass*, *Annals N.Y. Acad. Sci.* **375** (1981) 32 [SPIRES].

[6] J.R. Bond and A.S. Szalay, *The collisionless damping of density fluctuations in an expanding universe*, *Astrophys. J.* **274** (1983) 443 [SPIRES].

[7] L. Bergstrom, *Non-baryonic dark matter: observational evidence and detection methods*, *Rept. Prog. Phys.* **63** (2000) 793 [`hep-ph/0002126`] [SPIRES].

[8] G. Bertone, D. Hooper and J. Silk, *Particle dark matter: evidence, candidates and constraints*, *Phys. Rept.* **405** (2005) 279 [`hep-ph/0404175`] [SPIRES].

[9] J. Carr, G. Lamanna and J. Lavalle, *Indirect detection of dark matter*, *Rept. Prog. Phys.* **69** (2006) 2475 [SPIRES].

[10] M. Taoso, G. Bertone and A. Masiero, *Dark matter candidates: a ten-point test*, *JCAP* **03** (2008) 022 [`arXiv:0711.4996`] [SPIRES].

[11] S.L. Dubovsky, P.G. Tinyakov and I.I. Tkachev, *Massive graviton as a testable cold dark matter candidate*, *Phys. Rev. Lett.* **94** (2005) 181102 [`hep-th/0411158`] [SPIRES].

[12] F. Wilczek, *Problem of strong P and T invariance in the presence of instantons*, *Phys. Rev. Lett.* **40** (1978) 279 [SPIRES].

[13] S. Weinberg, *A new light boson?*, *Phys. Rev. Lett.* **40** (1978) 223 [SPIRES].

[14] R. Holman, G. Lazarides and Q. Shafi, *Axions and the dark matter of the universe*, *Phys. Rev.* **D 27** (1983) 995 [SPIRES].

[15] S. Dodelson and L.M. Widrow, *Sterile neutrinos as dark matter*, *Phys. Rev. Lett.* **72** (1994) 17 [`hep-ph/9303287`] [SPIRES].

[16] H. Pagels and J.R. Primack, *Supersymmetry, cosmology and new TeV physics*, *Phys. Rev. Lett.* **48** (1982) 223 [SPIRES].

[17] B.W. Lee and S. Weinberg, *Cosmological lower bound on heavy-neutrino masses*, *Phys. Rev. Lett.* **39** (1977) 165 [SPIRES].

[18] H.E. Haber and G.L. Kane, *The search for supersymmetry: probing physics beyond the Standard Model*, *Phys. Rept.* **117** (1985) 75 [SPIRES].

[19] L. Covi, J.E. Kim and L. Roszkowski, *Axinos as cold dark matter*, *Phys. Rev. Lett.* **82** (1999) 4180 [`hep-ph/9905212`] [SPIRES].

[20] L. Covi, H.-B. Kim, J.E. Kim and L. Roszkowski, *Axinos as dark matter*, *JHEP* **05** (2001) 033 [`hep-ph/0101009`] [SPIRES].

[21] A. Kusenko and M.E. Shaposhnikov, *Supersymmetric Q-balls as dark matter*, *Phys. Lett.* **B 418** (1998) 46 [`hep-ph/9709492`] [SPIRES].

[22] V. Kuzmin and I. Tkachev, *Ultra-high energy cosmic rays, superheavy long-living particles and matter creation after inflation*, *JETP Lett.* **68** (1998) 271 [`hep-ph/9802304`] [SPIRES].

[23] D.J.H. Chung, E.W. Kolb and A. Riotto, *Superheavy dark matter*, *Phys. Rev.* **D 59** (1999) 023501 [hep-ph/9802238] [SPIRES].

[24] S. Tremaine and J.E. Gunn, *Dynamical role of light neutral leptons in cosmology*, *Phys. Rev. Lett.* **42** (1979) 407 [SPIRES].

[25] A. Boyarsky, O. Ruchayskiy and D. Iakubovskyi, *A lower bound on the mass of dark matter particles*, *JCAP* **03** (2009) 005 [arXiv:0808.3902] [SPIRES].

[26] J. Madsen and R.I. Epstein, *Firm bounds on the neutrino mass from the distribution of dark matter in galaxies*, *Astrophys. J.* **282** (1984) 11 [SPIRES].

[27] J. Madsen, *Generalized Tremaîne-Gunn limits for bosons and fermions*, *Phys. Rev.* **D 44** (1991) 999 [SPIRES].

[28] J. Madsen, *Phase space constraints on bosonic and fermionic dark matter*, *Phys. Rev. Lett.* **64** (1990) 2744 [SPIRES].

[29] J.J. Dalcanton and C.J. Hogan, *Halo cores and phase space densities: observational constraints on dark matter physics and structure formation*, *Astrophys. J.* **561** (2001) 35 [astro-ph/0004381] [SPIRES].

[30] C.J. Hogan and J.J. Dalcanton, *New dark matter physics: clues from halo structure*, *Phys. Rev.* **D 62** (2000) 063511 [astro-ph/0002330] [SPIRES].

[31] J. Madsen, *Dark matter phase space densities*, *Phys. Rev.* **D 64** (2001) 027301 [astro-ph/0006074] [SPIRES].

[32] J. Madsen, *Dark matter phase space densities*, *Phys. Rev.* **D 64** (2001) 027301 [astro-ph/0006074] [SPIRES].

[33] D. Boyanovsky, H.J. de Vega and N. Sanchez, *Constraints on dark matter particles from theory, galaxy observations and N-body simulations*, *Phys. Rev.* **D 77** (2008) 043518 [arXiv:0710.5180] [SPIRES].

[34] D. Gorbunov, A. Khmelnitsky and V. Rubakov, *Constraining sterile neutrino dark matter by phase-space density observations*, *JCAP* **10** (2008) 041 [arXiv:0808.3910] [SPIRES].

[35] E. Kolb and M. Turner, *The early universe*, prepared with LaTeX, Addison-Wesley, Reading U.S.A. (1990).

[36] J.L. Feng, A. Rajaraman and F. Takayama, *Superweakly-interacting massive particles*, *Phys. Rev. Lett.* **91** (2003) 011302 [hep-ph/0302215] [SPIRES].

[37] F. Takayama and M. Yamaguchi, *Gravitino dark matter without R-parity*, *Phys. Lett.* **B 485** (2000) 388 [hep-ph/0005214] [SPIRES].

[38] W. Buchmüller, L. Covi, K. Hamaguchi, A. Ibarra and T. Yanagida, *Gravitino dark matter in R-parity breaking vacua*, *JHEP* **03** (2007) 037 [hep-ph/0702184] [SPIRES].

[39] J.P. Conlon and F. Quevedo, *Astrophysical and cosmological implications of large volume string compactifications*, *JCAP* **08** (2007) 019 [arXiv:0705.3460] [SPIRES].

[40] M. Lattanzi and J.W.F. Valle, *Decaying warm dark matter and neutrino masses*, *Phys. Rev. Lett.* **99** (2007) 121301 [arXiv:0705.2406] [SPIRES].

[41] A. Boyarsky, A. Neronov, O. Ruchayskiy, M. Shaposhnikov and I. Tkachev, *How to find a dark matter sterile neutrino?*, *Phys. Rev. Lett.* **97** (2006) 261302 [astro-ph/0603660] [SPIRES].

[42] G. Bertone, W. Buchmüller, L. Covi and A. Ibarra, *Gamma-rays from decaying dark matter*, *JCAP* **11** (2007) 003 [arXiv:0709.2299] [SPIRES].

[43] A. Boyarsky, A. Neronov, O. Ruchayskiy and M. Shaposhnikov, *Constraints on sterile neutrino as a dark matter candidate from the diffuse X-ray background*, *Mon. Not. Roy. Astron. Soc.* **370** (2006) 213 [astro-ph/0512509] [SPIRES].

[44] A. Boyarsky, A. Neronov, O. Ruchayskiy and M. Shaposhnikov, *Restrictions on parameters of sterile neutrino dark matter from observations of galaxy clusters*, *Phys. Rev.* **D 74** (2006) 103506 [astro-ph/0603368] [SPIRES].

[45] A. Boyarsky, J. Nevalainen and O. Ruchayskiy, *Constraints on the parameters of radiatively decaying dark matter from the dark matter halo of the milky way and ursa minor*, *Astron. Astrophys.* **471** (2007) 51 [astro-ph/0610961] [SPIRES].

[46] A. Boyarsky, O. Ruchayskiy and M. Markevitch, *Constraints on parameters of radiatively decaying dark matter from the galaxy cluster* 1*E*0657-56, *Astrophys. J.* **673** (2008) 752 [astro-ph/0611168] [SPIRES].

[47] A. Boyarsky, J.W. den Herder, A. Neronov and O. Ruchayskiy, *Search for the light dark matter with an X-ray spectrometer*, *Astropart. Phys.* **28** (2007) 303 [astro-ph/0612219] [SPIRES].

[48] P. Bode, J.P. Ostriker and N. Turok, *Halo formation in warm dark matter models*, *Astrophys. J.* **556** (2001) 93 [astro-ph/0010389] [SPIRES].

[49] L. Hui, N.Y. Gnedin and Y. Zhang, *The statistics of density peaks and the column density distribution of the Lyman-α forest*, *Astrophys. J.* **486** (1997) 599 [astro-ph/9608157] [SPIRES].

[50] N.Y. Gnedin and A.J.S. Hamilton, *Matter power spectrum from the Lyman-α forest: myth or reality?*, *Mon. Not. Roy. Astron. Soc.* **334** (2002) 107 [astro-ph/0111194] [SPIRES].

[51] D.H. Weinberg, R. Davé, N. Katz and J.A. Kollmeier, *The Lyman-α forest as a cosmological tool*, in *AIP Conf. Proc.* **666** (2003) 157, S.H. Holt and C.S. Reynolds eds., [astro-ph/0301186] [SPIRES].

[52] A.A. Meiksin, *The physics of the intergalactic medium*, arXiv:0711.3358 [SPIRES].

[53] M. Viel, M.G. Haehnelt, R.F. Carswell and T.S. Kim, *The effect of (strong) discrete absorption systems on the Lyman-α forest flux power spectrum*, *Mon. Not. Roy. Astron. Soc.* **349** (2004) L33 [astro-ph/0308078] [SPIRES].

[54] T.S. Kim, J.S. Bolton, M. Viel, M.G. Haehnelt and R.F. Carswell, *An improved measurement of the flux distribution of the Ly-α forest in QSO absorption spectra: the effect of continuum fitting, metal contamination and noise properties*, arXiv:0711.1862 [SPIRES].

[55] J.S. Bolton, M. Viel, T.S. Kim, M.G. Haehnelt and R.F. Carswell, *Possible evidence for an inverted temperature-density relation in the intergalactic medium from the flux distribution of the Lyman-α forest*, arXiv:0711.2064 [SPIRES].

[56] L. Gao and T. Theuns, *Lighting the universe with filaments*, *Science* **317** (2007) 1527 [arXiv:0709.2165] [SPIRES].

[57] P.L. Biermann and A. Kusenko, *Relic keV sterile neutrinos and reionization*, *Phys. Rev. Lett.* **96** (2006) 091301 [astro-ph/0601004] [SPIRES].

[58] J. Stasielak, P.L. Biermann and A. Kusenko, *Thermal evolution of the primordial clouds in warm dark matter models with keV sterile neutrinos*, *Astrophys. J.* **654** (2007) 290 [astro-ph/0606435] [SPIRES].

[59] C.A. Faucher-Giguere, J.X. Prochaska, A. Lidz, L. Hernquist and M. Zaldarriaga, *A direct precision measurement of the intergalactic Lyman-α opacity at* $2 < z < 4.2$, arXiv:0709.2382 [SPIRES].

[60] M. Viel, M.G. Haehnelt and V. Springel, *Inferring the dark matter power spectrum from the Lyman-α forest in high-resolution QSO absorption spectra*, *Mon. Not. Roy. Astron. Soc.* **354** (2004) 684 [astro-ph/0404600] [SPIRES].

[61] SDSS collaboration, P. McDonald et al., *The Lyman-α forest power spectrum from the Sloan digital sky survey*, *Astrophys. J. Suppl.* **163** (2006) 80 [astro-ph/0405013] [SPIRES].

[62] M. Viel and M.G. Haehnelt, *Cosmological and astrophysical parameters from the SDSS flux power spectrum and hydrodynamical simulations of the Lyman-α forest*, *Mon. Not. Roy. Astron. Soc.* **365** (2006) 231 [astro-ph/0508177] [SPIRES].

[63] M. Viel, J. Lesgourgues, M.G. Haehnelt, S. Matarrese and A. Riotto, *Constraining warm dark matter candidates including sterile neutrinos and light gravitinos with WMAP and the Lyman-α forest*, *Phys. Rev.* **D 71** (2005) 063534 [astro-ph/0501562] [SPIRES].

[64] U. Seljak, A. Makarov, P. McDonald and H. Trac, *Can sterile neutrinos be the dark matter?*, *Phys. Rev. Lett.* **97** (2006) 191303 [astro-ph/0602430] [SPIRES].

[65] M. Viel, J. Lesgourgues, M.G. Haehnelt, S. Matarrese and A. Riotto, *Can sterile neutrinos be ruled out as warm dark matter candidates?*, *Phys. Rev. Lett.* **97** (2006) 071301 [astro-ph/0605706] [SPIRES].

[66] M. Viel et al., *How cold is cold dark matter? Small scales constraints from the flux power spectrum of the high-redshift Lyman-α forest*, *Phys. Rev. Lett.* **100** (2008) 041304 [arXiv:0709.0131] [SPIRES].

[67] J.L. Feng, S.-F. Su and F. Takayama, *SuperWIMP gravitino dark matter from slepton and sneutrino decays*, *Phys. Rev.* **D 70** (2004) 063514 [hep-ph/0404198] [SPIRES].

[68] L. Roszkowski, R. Ruiz de Austri and K.-Y. Choi, *Gravitino dark matter in the CMSSM and implications for leptogenesis and the LHC*, *JHEP* **08** (2005) 080 [hep-ph/0408227] [SPIRES].

[69] D.G. Cerdeno, K.-Y. Choi, K. Jedamzik, L. Roszkowski and R. Ruiz de Austri, *Gravitino dark matter in the CMSSM with improved constraints from BBN*, *JCAP* **06** (2006) 005 [hep-ph/0509275] [SPIRES].

[70] K.-Y. Choi, J.E. Kim, H.M. Lee and O. Seto, *Neutralino dark matter from heavy axino decay*, *Phys. Rev.* **D 77** (2008) 123501 [arXiv:0801.0491] [SPIRES].

[71] M. Bolz, A. Brandenburg and W. Buchmüller, *Thermal production of gravitinos*, *Nucl. Phys.* **B 606** (2001) 518 [*Erratum ibid.* **B 790** (2008) 336] [hep-ph/0012052] [SPIRES].

[72] J. Pradler and F.D. Steffen, *Thermal gravitino production and collider tests of leptogenesis*, *Phys. Rev.* **D 75** (2007) 023509 [hep-ph/0608344] [SPIRES].

[73] V.S. Rychkov and A. Strumia, *Thermal production of gravitinos*, *Phys. Rev.* **D 75** (2007) 075011 [hep-ph/0701104] [SPIRES].

[74] S. Borgani, A. Masiero and M. Yamaguchi, *Light gravitinos as mixed dark matter*, *Phys. Lett.* **B 386** (1996) 189 [hep-ph/9605222] [SPIRES].

[75] T. Asaka, S. Blanchet and M. Shaposhnikov, *The nuMSM, dark matter and neutrino masses*, *Phys. Lett.* **B 631** (2005) 151 [hep-ph/0503065] [SPIRES].

[76] T. Asaka and M. Shaposhnikov, *The νMSM, dark matter and baryon asymmetry of the universe*, *Phys. Lett.* **B 620** (2005) 17 [hep-ph/0505013] [SPIRES].

[77] M. Shaposhnikov, *Is there a new physics between electroweak and Planck scales?*, arXiv:0708.3550 [SPIRES].

[78] X.-D. Shi and G.M. Fuller, *A new dark matter candidate: non-thermal sterile neutrinos*, *Phys. Rev. Lett.* **82** (1999) 2832 [astro-ph/9810076] [SPIRES].

[79] K. Abazajian, G.M. Fuller and M. Patel, *Sterile neutrino hot, warm and cold dark matter*, *Phys. Rev.* **D 64** (2001) 023501 [astro-ph/0101524] [SPIRES].

[80] T. Asaka, M. Laine and M. Shaposhnikov, *Lightest sterile neutrino abundance within the νMSM*, *JHEP* **01** (2007) 091 [hep-ph/0612182] [SPIRES].

[81] M. Laine and M. Shaposhnikov, *Sterile neutrino dark matter as a consequence of νMSM-induced lepton asymmetry*, *JCAP* **06** (2008) 031 [arXiv:0804.4543] [SPIRES].

[82] A.D. Dolgov and S.H. Hansen, *Massive sterile neutrinos as warm dark matter*, *Astropart. Phys.* **16** (2002) 339 [`hep-ph/0009083`] [SPIRES].

[83] M. Shaposhnikov, *The νMSM, leptonic asymmetries and properties of singlet fermions*, *JHEP* **08** (2008) 008 [`arXiv:0804.4542`] [SPIRES].

[84] A. Boyarsky, O. Ruchayskiy and M. Shaposhnikov, *The role of sterile neutrinos in cosmology and astrophysics*, `arXiv:0901.0011` [SPIRES].

[85] M. Shaposhnikov and I. Tkachev, *The νMSM, inflation and dark matter*, *Phys. Lett.* **B 639** (2006) 414 [`hep-ph/0604236`] [SPIRES].

[86] A. Kusenko, *Sterile neutrinos, dark matter and the pulsar velocities in models with a Higgs singlet*, *Phys. Rev. Lett.* **97** (2006) 241301 [`hep-ph/0609081`] [SPIRES].

[87] K. Petraki and A. Kusenko, *Dark-matter sterile neutrinos in models with a gauge singlet in the Higgs sector*, *Phys. Rev.* **D 77** (2008) 065014 [`arXiv:0711.4646`] [SPIRES].

[88] K. Petraki, *Small-scale structure formation properties of chilled sterile neutrinos as dark matter*, *Phys. Rev.* **D 77** (2008) 105004 [`arXiv:0801.3470`] [SPIRES].

[89] D. Boyanovsky, *Clustering properties of a sterile neutrino dark matter candidate*, *Phys. Rev.* **D 78** (2008) 103505 [`arXiv:0807.0646`] [SPIRES].

[90] A. Palazzo, D. Cumberbatch, A. Slosar and J. Silk, *Sterile neutrinos as subdominant warm dark matter*, *Phys. Rev.* **D 76** (2007) 103511 [`arXiv:0707.1495`] [SPIRES].

[91] M. Viel, M.G. Haehnelt and V. Springel, *Inferring the dark matter power spectrum from the Lyman-α forest in high-resolution QSO absorption spectra*, *Mon. Not. Roy. Astron. Soc.* **354** (2004) 684 [`astro-ph/0404600`] [SPIRES].

[92] SDSS collaboration, P. McDonald et al., *The linear theory power spectrum from the Lyman-α forest in the Sloan digital sky survey*, *Astrophys. J.* **635** (2005) 761 [`astro-ph/0407377`] [SPIRES].

[93] S. Colombi, S. Dodelson and L.M. Widrow, *Large scale structure tests of warm dark matter*, *Astrophys. J.* **458** (1996) 1 [`astro-ph/9505029`] [SPIRES].

[94] J. Lesgourgues and S. Pastor, *Massive neutrinos and cosmology*, *Phys. Rept.* **429** (2006) 307 [`astro-ph/0603494`] [SPIRES].

[95] A. Lewis, A. Challinor and A. Lasenby, *Efficient computation of CMB anisotropies in closed FRW models*, *Astrophys. J.* **538** (2000) 473 [`astro-ph/9911177`] [SPIRES].

[96] W. Hu, D.J. Eisenstein and M. Tegmark, *Weighing neutrinos with galaxy surveys*, *Phys. Rev. Lett.* **80** (1998) 5255 [`astro-ph/9712057`] [SPIRES].

[97] H. Bi *Lyman-α absorption spectrum of the primordial intergalactic medium*, *Astrophys. J.* **405** (1993) 479.

[98] M. Viel, S. Matarrese, H.J. Mo, M.G. Haehnelt and T. Theuns, *Probing the intergalactic medium with the Lyman-α forest along multiple lines of sight to distant QSOs*, *Mon. Not. Roy. Astron. Soc.* **329** (2002) 848 [`astro-ph/0105233`] [SPIRES].

[99] M. Zaldarriaga, R. Scoccimarro and L. Hui, *Inferring the linear power spectrum from the Lyman-α forest*, *Astrophys. J.* **590** (2003) 1 [`astro-ph/0111230`] [SPIRES].

[100] A. Lewis and S. Bridle, *Cosmological parameters from CMB and other data: a Monte-Carlo approach*, *Phys. Rev.* **D 66** (2002) 103511 [`astro-ph/0205436`] [SPIRES].

[101] T. Theuns, A. Leonard, G. Efstathiou, F.R. Pearce and P.A. Thomas, *P^3M-SPH simulations of the Lyman-α forest*, *Mon. Not. Roy. Astron. Soc.* **301** (1998) 478 [`astro-ph/9805119`] [SPIRES].

[102] M. Viel, M.G. Haehnelt and V. Springel, *Testing the accuracy of the Hydro-PM approximation in numerical simulations of the Lyman-α forest*, *Mon. Not. Roy. Astron. Soc.* **367** (2006) 1655 [astro-ph/0504641] [SPIRES].

[103] J.A. Regan, M.G. Haehnelt and M. Viel, *Numerical simulations of the Lyman-α forest — a comparison of Gadget-2 and Enzo*, *Mon. Not. Roy. Astron. Soc.* **374** (2007) 196 [astro-ph/0606638] [SPIRES].

[104] T.S. Kim, M. Viel, M.G. Haehnelt, R.F. Carswell and S. Cristiani, *The power spectrum of the flux distribution in the Lyman-α forest of a large sample of UVES QSO absorption spectra (LUQAS)*, *Mon. Not. Roy. Astron. Soc.* **347** (2004) 355 [astro-ph/0308103] [SPIRES].

[105] R.A.C. Croft et al., *Towards a precise measurement of matter clustering: Lyman-α forest data at redshifts* 2-4, *Astrophys. J.* **581** (2002) 20 [astro-ph/0012324] [SPIRES].

[106] N.Y. Gnedin and L. Hui, *Probing the universe with the Lyman-α forest: i. Hydrodynamics of the low density IGM*, *Mon. Not. Roy. Astron. Soc.* **296** (1998) 44 [astro-ph/9706219] [SPIRES].

[107] SDSS collaboration, M. Bernardi et al., *A feature at $z \sim 3.2$ in the evolution of the Lyα forest optical depth*, *Astron. J.* **125** (2003) 32 [astro-ph/0206293] [SPIRES].

[108] P. McDonald, U. Seljak, R. Cen, P. Bode and J.P. Ostriker, *Physical effects on the Lyman-α forest flux power spectrum: damping wings, ionizing radiation fluctuations and galactic winds*, *Mon. Not. Roy. Astron. Soc.* **360** (2005) 1471 [astro-ph/0407378] [SPIRES].

[109] E. Bertschinger, *COSMICS: cosmological initial conditions and microwave anisotropy codes*, astro-ph/9506070 [SPIRES].

[110] A. Klypin and J. Holtzman, *Particle-mesh code for cosmological simulations*, astro-ph/9712217 [SPIRES].

[111] A. Klypin, *Numerical simulations in cosmology I: methods*, astro-ph/0005502 [SPIRES].

[112] V. Springel, *The cosmological simulation code GADGET-2*, *Mon. Not. Roy. Astron. Soc.* **364** (2005) 1105 [astro-ph/0505010] [SPIRES].

[113] P. Colín, O. Valenzuela and V. Avila-Reese, *On the structure of dark matter halos at the damping scale of the power spectrum with and without relict velocities*, *Astrophys. J.* **673** (2008) 203 [arXiv:0709.4027] [SPIRES].

[114] WMAP collaboration, J. Dunkley et al., *Five-year Wilkinson Microwave Anisotropy Probe (WMAP) observations: likelihoods and parameters from the WMAP data*, *Astrophys. J. Suppl.* **180** (2009) 306 [arXiv:0803.0586] [SPIRES].

[115] ACBAR collaboration, C.-l. Kuo et al., *High resolution observations of the CMB power spectrum with ACBAR*, *Astrophys. J.* **600** (2004) 32 [astro-ph/0212289] [SPIRES].

[116] A.C.S. Readhead et al., *Extended mosaic observations with the cosmic background imager*, *Astrophys. J.* **609** (2004) 498 [astro-ph/0402359] [SPIRES].

[117] F. Piacentini et al., *A measurement of the polarization-temperature angular cross power spectrum of the cosmic microwave background from the* 2003 *flight of BOOMERANG*, *Astrophys. J.* **647** (2006) 833 [astro-ph/0507507] [SPIRES].

[118] W.C. Jones et al., *A measurement of the angular power spectrum of the CMB temperature anisotropy from the* 2003 *flight of boomerang*, *Astrophys. J.* **647** (2006) 823 [astro-ph/0507494] [SPIRES].

[119] T.E. Montroy et al., *A measurement of the CMB $\langle EE \rangle$ spectrum from the* 2003 *flight of BOOMERANG*, *Astrophys. J.* **647** (2006) 813 [astro-ph/0507514] [SPIRES].

[120] C.J. MacTavish et al., *Cosmological parameters from the* 2003 *flight of BOOMERANG*, *Astrophys. J.* **647** (2006) 799 [astro-ph/0507503] [SPIRES].

[121] SDSS collaboration, M. Tegmark et al., *Cosmological constraints from the SDSS luminous red galaxies*, *Phys. Rev.* **D 74** (2006) 123507 [`astro-ph/0608632`] [SPIRES].

[122] THE SNLS collaboration, P. Astier et al., *The supernova legacy survey: measurement of* Ω_M, Ω_Λ *and w from the first year data set*, *Astron. Astrophys.* **447** (2006) 31 [`astro-ph/0510447`] [SPIRES].

[123] U. Seljak, P. McDonald and A. Makarov, *Cosmological constraints from the CMB and Lyman-α forest revisited*, *Mon. Not. Roy. Astron. Soc.* **342** (2003) L79 [`astro-ph/0302571`] [SPIRES].

[124] N.Y. Gnedin and L. Hui, *Probing the universe with the Lyman-α forest: i. Hydrodynamics of the low density IGM*, *Mon. Not. Roy. Astron. Soc.* **296** (1998) 44 [`astro-ph/9706219`] [SPIRES].

[125] D. Tytler, P. Paschos, D. Kirkman, M.L. Norman and T. Jena, *How simulated spectra of the Lyman-α forest change with the size of the box of numerical simulations*, `arXiv:0711.2529` [SPIRES].

[126] R.A.C. Croft, *Ionizing radiation fluctuations and large-scale structure in the Lyman-α forest*, *Astrophys. J.* **610** (2004) 642 [`astro-ph/0310890`] [SPIRES].

[127] M. Jubelgas, V. Springel, T. Enßlin and C. Pfrommer, *Cosmic ray feedback in hydrodynamical simulations of galaxy formation*, *Astron. Astrophys.* **481** (2008) 33 [`astro-ph/0603485`] [SPIRES].

[128] T. Asaka, M. Laine and M. Shaposhnikov, *On the hadronic contribution to sterile neutrino production*, *JHEP* **06** (2006) 053 [`hep-ph/0605209`] [SPIRES].

[129] A. Boyarsky, D. Iakubovskyi, O. Ruchayskiy and V. Savchenko, *Constraints on decaying dark matter from XMM-Newton observations of M31*, *Mon. Not. Roy. Astron. Soc.* **387** (2008) 1361 [`arXiv:0709.2301`] [SPIRES].

[130] S. Riemer-Sorensen, S.H. Hansen and K. Pedersen, *Sterile neutrinos in the Milky Way: observational constraints*, *Astrophys. J.* **644** (2006) L33 [`astro-ph/0603661`] [SPIRES].

[131] C.R. Watson, J.F. Beacom, H. Yuksel and T.P. Walker, *Direct X-ray constraints on sterile neutrino warm dark matter*, *Phys. Rev.* **D 74** (2006) 033009 [`astro-ph/0605424`] [SPIRES].

[132] K.N. Abazajian, M. Markevitch, S.M. Koushiappas and R.C. Hickox, *Limits on the radiative decay of sterile neutrino dark matter from the unresolved cosmic and soft X-ray backgrounds*, *Phys. Rev.* **D 75** (2007) 063511 [`astro-ph/0611144`] [SPIRES].

[133] A. Boyarsky, J. Lesgourgues, O. Ruchayskiy and M. Viel, *Realistic sterile neutrino dark matter with keV mass does not contradict cosmological bounds*, `arXiv:0812.3256` [SPIRES].

[134] D. Tytler et al., *Cosmological parameters* σ_8, *the baryon density* ω_b, *the Vacuum Energy Density* ω_Λ, *the Hubble Constant and the UV background intensity from a calibrated measurement of H I Lyα absorption at* $z = 1.9$, *Astrophys. J.* **617** (2004) 1 [`astro-ph/0403688`] [SPIRES].

[135] L. Kaper, S. D'Odorico, F. Hammer, R. Pallavicini and P.K. Rasmussen, *X-shooter: a medium-resolution, wide-band spectrograph for the VLT*, `arXiv:0803.0609` [SPIRES].

[136] D.J.C. MacKay, *Information theory, inference and learning algorithms*, Cambridge University Press, Cambridge U.K. (2003), http://www.inference.phy.cam.ac.uk/mackay/itprnn/book.html.

[137] G.J. Feldman and R.D. Cousins, *A unified approach to the classical statistical analysis of small signals*, *Phys. Rev.* **D 57** (1998) 3873 [`physics/9711021`] [SPIRES].

[138] D. Karlen, *Credibility of confidence intervals*, prepared for *Conference on Advanced Statistical Techniques in Particle Physics, Durham U.K. March* 18–22 2002 [SPIRES].

– 41 –

[139] A. Kosowsky, M. Milosavljevic and R. Jimenez, *Efficient cosmological parameter estimation from microwave background anisotropies*, *Phys. Rev.* **D 66** (2002) 063007 [astro-ph/0206014] [SPIRES].

[140] J. Dunkley, M. Bucher, P.G. Ferreira, K. Moodley and C. Skordis, *Fast and reliable MCMC for cosmological parameter estimation*, *Mon. Not. Roy. Astron. Soc.* **356** (2005) 925 [astro-ph/0405462] [SPIRES].

[141] R. Trotta, *Bayes in the sky: bayesian inference and model selection in cosmology*, *Contemp. Phys.* **49** (2008) 71 [arXiv:0803.4089] [SPIRES].

[142] R.M. Neal, *Probabilistic inference using Markov chain Monte Carlo methods*, http://cosmologist.info/Neal93, (1993).